INSTRUMENTATION AND CALIBRATION OF X-RAY SCINTILLATION PAIR SPECTROMETER

Joseph Edward Synder, Jr.

INSTRUMENTATION AND CALIBRATION OF X-RAY SCINTILLATION PAIR SPECTROMETER

by

Joseph Edward Snyder, Jr.
B.S., United States Naval Academy
(1944)

Submitted in Partial Fulfillment of the

Requirements for the Degree of

MASTER OF SCIENCE

at the

MASSACHUSETTS INSTITUTE OF TECHNOLOGY
(1955)

Signature of Author_____
Department of Physics, May 23, 1955

Certified by_____
Thesis Supervisor

Accepted by_____
Chairman, Departmental Committee on Graduate Students

INSTRUMENTATION AND CALIBRATION OF

X-RAY SCINTILLATION PAIR SPECTROMETER

by

Joseph Edward Snyder, Jr.

Submitted to the Department of Physics on May 23, 1955 in partial fulfillment of the requirements for the degree of Master of Science.

ABSTRACT

This paper describes an x-ray spectrometer designed for use at the M.I.T. linear accelerator. The spectrometer is a three-counter telescope with a thin lead radiator between the first and second counter. The first and second counters are thin plastic scintillators; the third, a thick plastic scintillator. An acceptable event is one in which there is no pulse in the first counter and a doubly ionizing pulse in the second counter in coincidence with the third counter. Such events should be electron-positron pairs originating only in the radiator. To a first approximation, the sum of the pulse heights produced in the second and third counter is proportional to the incident x-ray energy.

Thesis Supervisor: Bernard T. Feld

Title: Associate Professor of Physics

Polymerization and Calibration of
P-Bit Scintillation Mix Encapsulants

by

Nancy Simmons Duprey, Ab.

Submitted to the Department of Physics on May 21, 1905 in partial fulfillment of the requirements for the degree of Doctor of Science.

Abstract

This paper describes an energy resolution designed for use at the M.I.T. Linear Accelerator. The scintillator is a three-quarter batteries with a thin lead radiator between the first and second counters. The first and second coincidents are fully plastic scintillators, the third, a thick plastic scintillator. In operation events in the third, where it has passed through both lower counters, produce in the second counter a pulse proportional to the total energy. Such events should be distinguishable from lower energy events produced in the second and third counter by pulse height discrimination. To a first approximation, the ratio of the pulse heights produced in the second and third counter is proportional to the incident energy.

Thesis Supervisor: Norman T. Peña

Title: Associate Professor of Physics

TABLE OF CONTENTS

TABLE OF CONTENTS

LIST OF ILLUSTRATIONS

List of Illustrations

ACKNOWLEDGMENTS

The author* expresses his appreciation to all those who have helped to make this work possible. He is particularly indebted to Dr. P. T. Demos for friendly guidance and helpful advice throughout the course of this and other work; to Dr. C. P. Sargent for active participation in all phases of the experimental work; to Professor R. D. Evans and Professor B. T. Feld for advice in various phases of the experiment and theory; to Dr. Hans Mark for making the facilities of the Rockefeller generator available and for many other kindnesses and helpful suggestions; to Mr. H. W. Greene for help in the construction of the electronic components.

For the typing and proofreading, the author would like to express his special thanks to Mrs. Mary E. White. Thanks are also due Mrs. Grace Rowe for making the drawings and to Mr. N. Saia for making the block diagrams.

*Enrolled at the Massachusetts Institute of Technology under the United States Naval Postgraduate School system through the sponsorship of the Bureau of Ordnance, Navy Department.

ACKNOWLEDGMENT

The author expresses his appreciation to all those who have helped to make this work possible. He is particularly indebted to Dr. F. T. Thwaites for friendly guidance and helpful advice throughout the course of this and other work; to Dr. C. P. Haagsma for active participation in all phases of the experimental work; to Professor E. D. Evans and Professor S. T. Field for advice in various phases of the experimental and theory; to Dr. Alma Mack for making the facilities of the Nuclear Laboratory available and for many other kindnesses and helpful suggestions; to Mr. T. Symons for help in the construction of the electronic components.

For the typing and proofreading, the author would like to express his special thanks to Mrs. Mary E. White. Thanks are also due Mrs. Thrune Lowe for making the drawings and to Mr. E. Mack for making the black diagrams.

Supported as the Massachusetts Institute of Technology under the United States Naval Postgraduate School program through the generosity of the Bureau of Ordnance, Navy Department.

I. INTRODUCTION

The intention of this paper is to describe an x-ray spectrometer designed for use at the M. I. T. linear accelerator. The spectrometer is a three-counter telescope with a thin lead radiator between the first and second counter. The first and second counters are thin plastic scintillators; the third, a thick plastic scintillator. An acceptable event is one in which there is no pulse in the first counter and a doubly ionizing pulse in the second counter in coincidence with the third counter. Such events should be electron-positron pairs originating only in the radiator. To a first approximation, the sum of the pulse heights produced in the second and third counter is proportional to the incident x-ray energy. This chapter is devoted to explaining the need for a spectrometer of this type at the linear accelerator.

Five- to 25-Mev x-rays are known to interact strongly with nuclei. Among the heavier elements, as much as 2 percent of the total absorption coefficient for 25-Mev bremsstrahlung is of nuclear rather than atomic origin. Most of the experiments have investigated the emission of heavy particles following photon absorption. Recently, however, some measurements have been made of nuclear absorption coefficients in good geometry transmission experiments[1] and of large-angle scattering of bremsstrahlung[2].

1. INTRODUCTION

The intention of this paper is to describe an x-ray spectrometer designed for use at the M. I. T. Linear Accelerator. The spectrometer is a three-counter telescope with a thin lead radiator between the first and second counters. The first and second counters are thin plastic scintillators; the third, a thick plastic scintillator. An acceptable event is one in which there is no pulse in the first counter and a definite incoming pulse in the second counter in coincidence with the third counter. Such events should be electron-positron pairs originating only in the radiator. To a first approximation, the sum of the pulse heights produced in the second and third counter is proportional to the incident x-ray energy. This chapter is devoted to explaining the need for a spectrometer of this type at the linear accelerator.

Pions in 70-Mev x-rays are known to interact strongly with nuclei. Among the heavier elements, as much as 2 percent of the total absorption coefficient for 70-Mev bremsstrahlung is of nuclear rather than atomic origin. Most of the experiments have investigated the existence of heavy mesotrons following absorption. Recently, however, some experiments have been made of nuclear absorption coefficients in good counter transmission experiments[1] and of integral angle coefficients of bremsstrahlung[2].

The M. I. T. linear accelerator is 10 to 100 times as strong a source of 5- to 17-Mev x-rays as the usual betatron of comparable energy. This accelerator can furnish average electron currents of about 2 microamperes. It is, however, a pulsed machine with a duty ratio of only 10^{-4}, and during the 1 microsecond pulse, the current reaches peaks of about 50 milliamperes. The low-duty ratio of the accelerator is a very important factor in the design of an x-ray spectrometer for use at the M.I.T. linear accelerator. The counting rate of a detector can be no more than a few counts per second, and the detector must be able to operate in the presence of a very high level of background radiation (low-energy photons and fast neutrons) present during the 1 microsecond pulse. One must use this high photon intensity of the accelerator to obtain energy resolution, good geometry, or small target size, rather than to obtain high counting rates.

A second limitation of the M. I. T. linear accelerator as a photon source imposes further restrictions on a photon detector. The electron energy spectrum of the accelerator is not only far from monochromatic, but it is difficult to keep the spectrum constant during a run and difficult to reproduce the same spectrum on subsequent runs. If one is to use all the current available and, say, thick-target bremsstrahlung in order to make as strong a photon source as possible, it is:

1. Necessary to monitor the photon spectrum itself rather than the electron current; and

The S. L. C. linear accelerator is 10 to 100 times as strong a source of 1- to 17-Bev energy as the usual betatron of comparable energy. This accelerator can furnish average electron currents of about 2 microamperes. It is, however, a pulsed machine with a duty ratio of only 10^{-4}, and during the 1 microsecond pulse, the current reaches peaks of about 20 milliamperes. The low-duty ratio of the accelerator is a very important factor in the design of an x-ray apparatus for use at the S.L.C. linear accelerator. The operating rate of a detector may be no more than a few counts per second, and the detector must be able to operate in the presence of a very high level of background radiation (low-energy electron and fast neutron) produced during the 1 microsecond pulse. One must use this high photon intensity of the accelerator to obtain energy resolution, good geometry, or small target size, rather than to obtain high counting rates.

A second limitation of the S. L. C. linear accelerator as a photon source imposes further restrictions on a photon detector. The electron energy fluctuations of the accelerator is not only for fractions of a per cent difficult to improve the beam dynamics as subsequent runs. If one is to use all the current available and, say, obtain targets bombarding in order to gain an strength a photon source as possible, it is:

1. Necessary to monitor the photon spectrum itself rather than the electron current; and

2. Very desirable to obtain as much information as possible from a single run.

The most efficient photon detector with reasonable resolution is a large volume of NaI. Such a spectrometer has been constructed by Koch[3]. Koch's best detector is a total absorption spectrometer with 11 percent resolution at 11 Mev, employing a NaI crystal 5 x 8 inches. His 2 x 2 x 5-inch NaI crystal gives about 20 percent resolution at 10 Mev. For use at the accelerator, the expense of such a large amount of NaI would perhaps be justified were it not for

1. The extreme sensitivity of NaI to photon radiation;
2. Its relative slow decay time of about 0.3 μ sec.

The first limitation requires the spectrometer to be enclosed in a massive amount of shielding. In a large-angle photon scattering experiment, the signal would need to be clipped to a fraction of the decay time of NaI to reduce pile-up of Compton recoil electrons. The differential cross section for Compton scattering at 90 degrees is as much as 10^5 times as large as cross sections one would like to measure, and the pile-up of the approximately half Mev Compton scattered photons during the 1 μ second accelerator pulse is a serious problem with any photon detector which involves pulse-height analysis.

The best energy resolution in the 5- to 17-Mev region is obtained with a magnetic pair spectrometer. Walker and McDaniel[4] were among the first in this field and obtained a solid angle times efficiency of approximately 10^{-7} with an energy resolution (width at half

2. They desirable to obtain as much information as possible from a single run.

The most efficient photon detector with reasonable resolution is a large volume of NaI. Such a spectrometer has been constructed by Kane[3]. Kane's best detector is a total absorption spectrometer with 12 percent resolution at 12 Mev, employing a NaI crystal 5 x 8 inches. His 5 x 5 x 5-inch NaI crystal gives about 20 percent resolution at 10 Mev. For use at the accelerator, the expense of such a large amount of NaI would perhaps be justified were it not for

1. The extreme sensitivity of NaI to photon radiation;

2. The relative slow decay time of about 0.3 μ sec.

The first limitation requires the spectrometer to be enclosed in a massive amount of shielding. In a large-angle photon scattering experiment, the signal would need to be clipped to a fraction of the decay time of NaI to reduce pile-up of Compton recoil electrons. The differential cross section for Compton scattering at 90 degrees is such as to[4] times as large as energy resolution one would like to measure, and the fluxes of the synchrotron itself may create unwanted photons during the 1 μ second accelerator pulse is a serious problem with any photon detector which involves pulse-height analysis.

The best energy resolutions in the 5- to 17-Mev region is obtained with a magnetic pair spectrometer. Fuller and McDaniel[5] were among the first in this field and obtained a solid angle times efficiency of approximately 10^{-7} with an energy resolution (width at half

maximum) of 5.5 percent. Currently, the best energy resolution in the 5- to 17-Mev energy range is obtained by Kinsey and Bartholomew[5], using a similar improved version of Walker and McDaniel's magnetic pair spectrometer. Using a 4.7 milligram/cm^2 gold radiator, Kinsey's best half-width is 140 kev, independent of photon energy.

The linear accelerator is a sufficiently strong source of x-rays to enable one to utilize a high-resolution, low-efficiency magnetic pair spectrometer. It should be able to measure the entire energy spectrum at one time; hence, it would have many channels and be of large size.

Another type of spectrometer, known as the three-crystal scintillation spectrometer[6-8], employing three NaI 1-1/2 inch diameter crystals proves useful in the 4- to 12-Mev energy range. A typical arrangement[6] employs two 1-1/2 inch by 1 inch thick NaI crystals as annihilation radiation detectors and a center 1-1/2 inch by 4 inch long NaI crystal which measures the energy of the coincidence pair. Counter efficiency at 6 Mev is about 10^{-5}, and width at half maximum is 7 percent.

Energy resolution with this three-crystal scintillation spectrometer at 11 Mev is 11 percent. In addition to those limitations imposed by the linear accelerator on the NaI total absorption spectrometer, the three-crystal scintillation spectrometer depends on 0.51-Mev photons in coincidence for its resolution, and hence is not easily adaptable for use at the M.I.T. linear accelerator.

maximum) of 7.6 percent. Currently, the best energy resolution in the 5- to 17-Mev energy range is obtained by Kinsey and Bartholomew[5], using a slightly improved version of Walker and Deutsch's magnetic resonance. Using a 5.7 milligram/cm^2 gold radiator, Kinsey's best half-width is 180 kev, independent of photon energy.

The linear accelerator is a particularly strong source of x-rays to enable one to utilize a high-resolution, low-efficiency magnetic pair spectrometer. It should be able to measure the entire energy spectrum at one time; hence, it would have many channels and be of large size.

Another type of spectrometer, known as the three-crystal scintillation spectrometer[6], employing three NaI 1-1/2 inch diameter crystals proves useful in the 4- to 12-Mev energy range. A typical arrangement[6] employs two 1-1/2 inch by 1 inch thick NaI crystals as annihilation radiation detectors and a center 1-1/2 inch by 4 inch long NaI crystal which measures the energy of the entering pair. Counter efficiency at 6 Mev is about 10^{-5}, and width at half maximum is 7 percent.

Energy resolution with this three-crystal scintillation spectrometer at 11 Mev is 11 percent. In addition to those limitations imposed by the linear accelerator as the NaI total absorption spectrometer, the three-crystal scintillation spectrometer depends on 0.51-Mev photons to coincidence for its resolution, and hence is not easily adaptable for use at the M.I.T. linear accelerator.

A fourth approach to the problem has been attempted, which should provide:

1. Approximately 10 percent resolution at 10 Mev;

2. Small dimensions and ease of shielding;

3. Solid-angle times efficiency of about 10^{-4};

4. Ability to measure an entire spectrum of photons from 5- to 17-Mev at a single run with several bins per resolution width;

5. Simplicity and economy as far as the actual detection is concerned. The major investment would go into the design and construction of associated electronic equipment. This same equipment would be useful for other projects at the M. I. T. accelerator (see, for example, W. J. Sawtelle, S.M. Thesis, M.I.T., May 1955).

II. APPARATUS

DESCRIPTION OF SPECTROMETER

The spectrometer scintillators are commercially available "Pilot B" crystals, density 1.03, polyvinyl toluene, para-terphenyl, para-para-prime diphenylstilbene[19]. Preliminary measurements indicate a decay time of less than 3×10^{-9} seconds[20]. Figure 1 shows to scale the physical arrangement of the spectrometer. The beam of photons from the source being surveyed is collimated by means of a half-inch hole in a 3-inch thick lead disk. The collimated photons are then incident on a lead foil where they interact forming pairs and Compton recoil electrons. This foil is known as the "converter." The converter is one-half inch in diameter, cemented to a thin lucite ring. The converter fits flush against scintillator No. 2, which in turn is held flush against scintillator No. 1. No. 2 scintillator is a cylinder 3/4 inch in diameter by 3/16 inch thick; No. 1 scintillator is a tapered cylinder 3 inches long, tapering from 2-1/4 inches in diameter to 1-1/2 inches in diameter one-half inch from the end. Figure 2 shows the shape and arrangement of the plastic scintillators.

Scintillator No. 1 has all its open faces wrapped in 1-mil aluminum foil to improve the light collection and to separate optically scintillator No. 1 from scintillator No. 2. The scintillation unit comprises the plastic scintillator, optical coupling, and selected RCA 5819 phototube. Figure 3 shows to scale the method of construction of unit No. 1.

12. APPARATUS

Commercial Equipment

The spectrophotometer principally used was commercially available "Coleman 11" recording, double 1.0% collimated beam, grating-prism-grating diffraction instrument[19]. The illuminant was a hydrogen discharge tube operated by a 10-kc power supply[20]. Figure 1 shows by vertical cross-section the arrangement of the spectrometer. The beam of photons from the source is collimated by means of a half-inch hole in a 3-inch brass lead disk. The collimated photons are then deflected on a lead foil whose blue fluorescent coating cuts out the unwanted ultraviolet. This foil is known as the "deflector." The deflector is one-half inch in diameter, mounted to a brass handle which is held firmly against polarizer No. 2, which is in a position 3/4 inch in diameter by 3/32 inch thick; No. 2 polarizer is kept in a constant position 3 inches long, measured from 2-1/2 inches in diameter to 3-1/2 inches in diameter one-half inch from the end. Figure 2 shows this plate and arrangement of the plastic polarizers.

Polarizer No. 1 has all the open faces covered to 1-mil aluminum foil to remove the light reflections and to accurately polarize No. 1 from polarizer No. 2. The polarizing sheets comprise the plastic polarizer, optical coupling, and mounted FCA 6710 plastics. Figure 3 shows in scale the method of construction of unit No. 1.

Figure 1

Physical Arrangement of the Spectrometer

The axis of scintillator unit No. 3 is perpendicular to both the axis of unit No. 2 and unit No. 1.

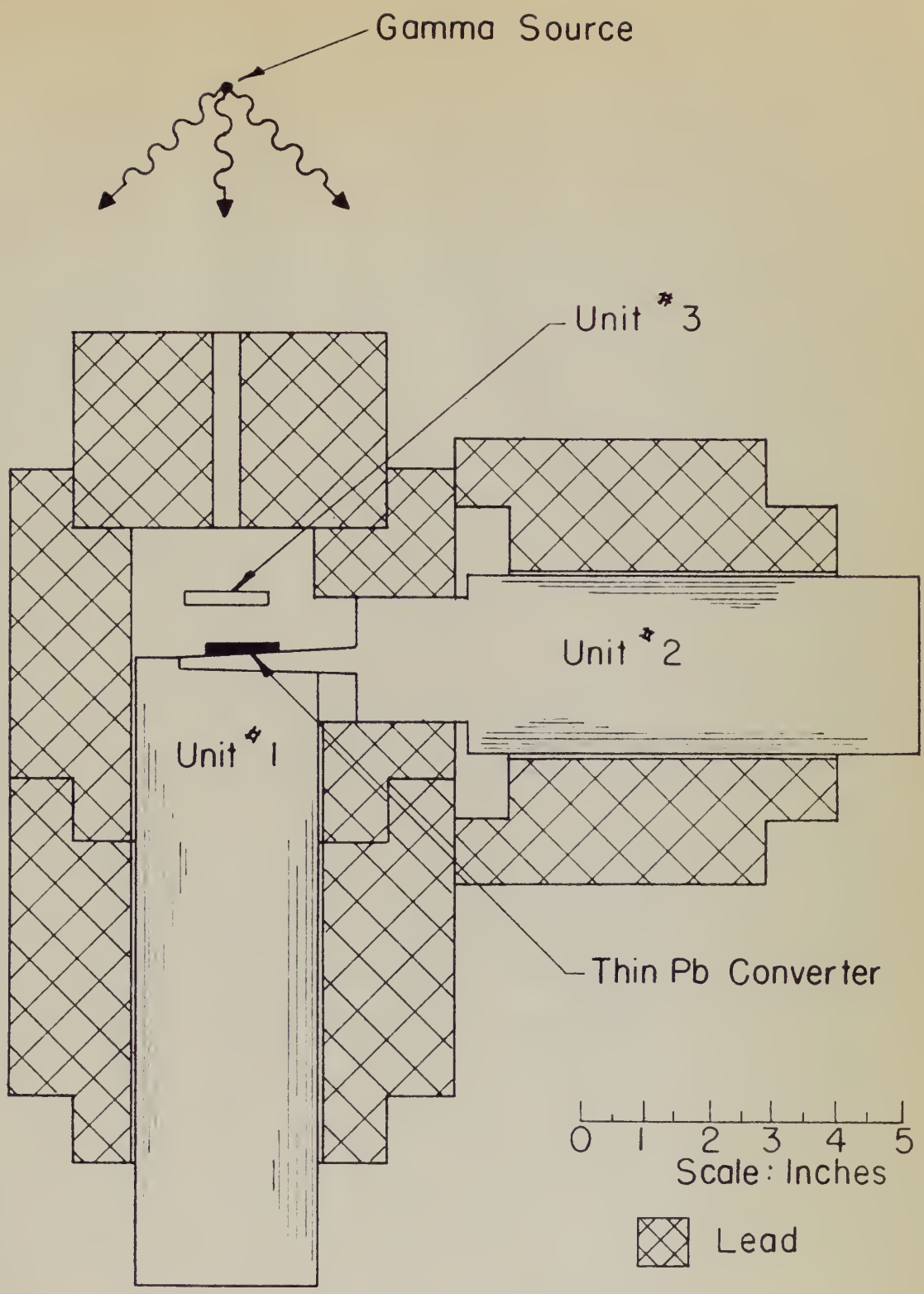

SHIELDING ARRANGEMENT

Figure 2

Arrangement and Shape of the
Plastic Ventilators

Plastic ventilator No. 2 is a push fit into the Insite light pipe. The converter, No. 3 ventilator, and ventilator No. 1 are held together by a clamp arrangement.

Figure 2

Arrangement and Shapes of the
Plastic Scintillators

Plastic scintillator No. 2 is a push fit into the lucite light pipe. The converter, No. 2 scintillator, and scintillator No. 1 are held together by a clamp arrangement.

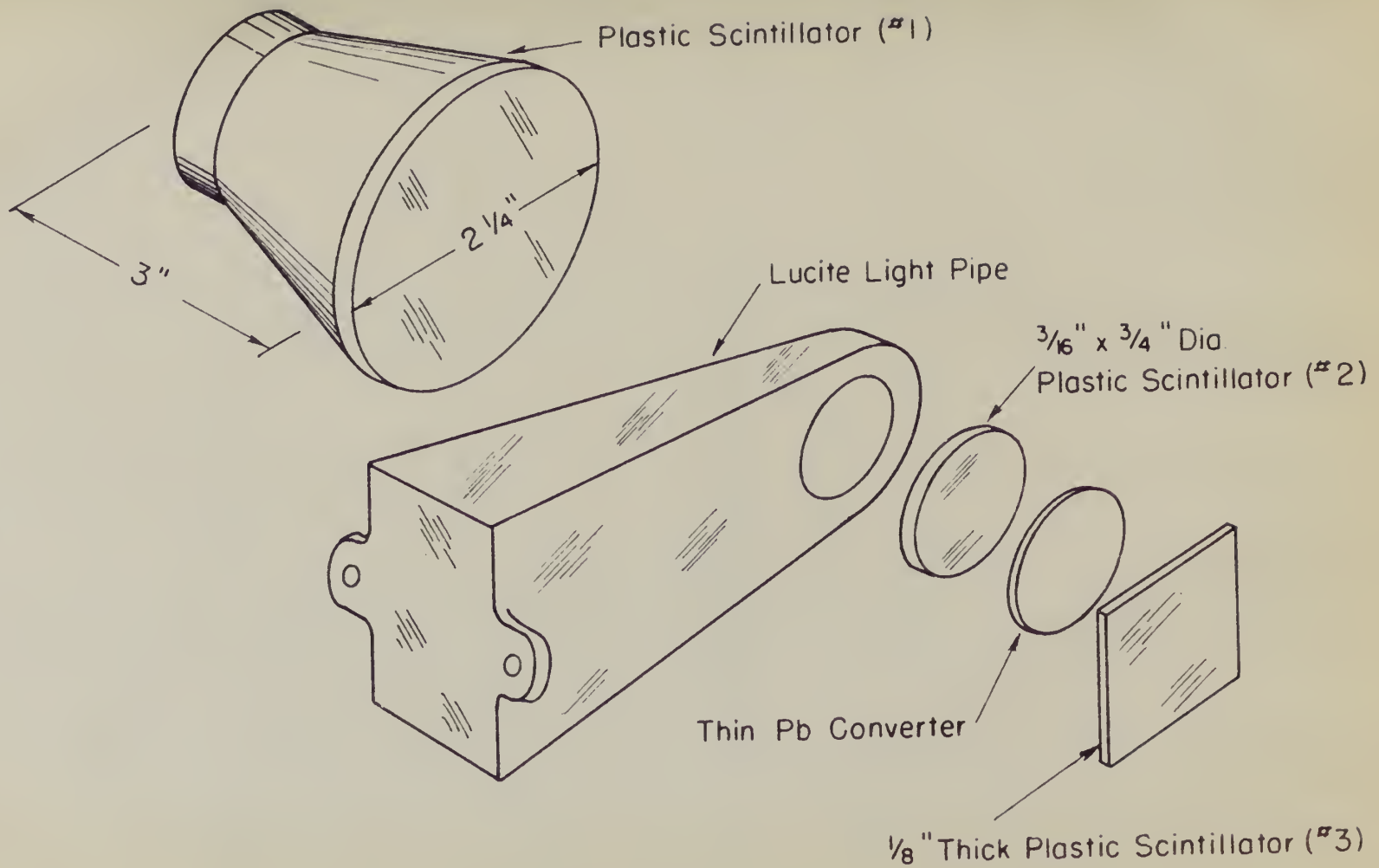

ARRANGEMENT OF PLASTIC SCINTILLATORS

Figure 3

Construction of Scintillation Unit No. 1.

Figure 3

Construction of Ventilation Unit No. 1.

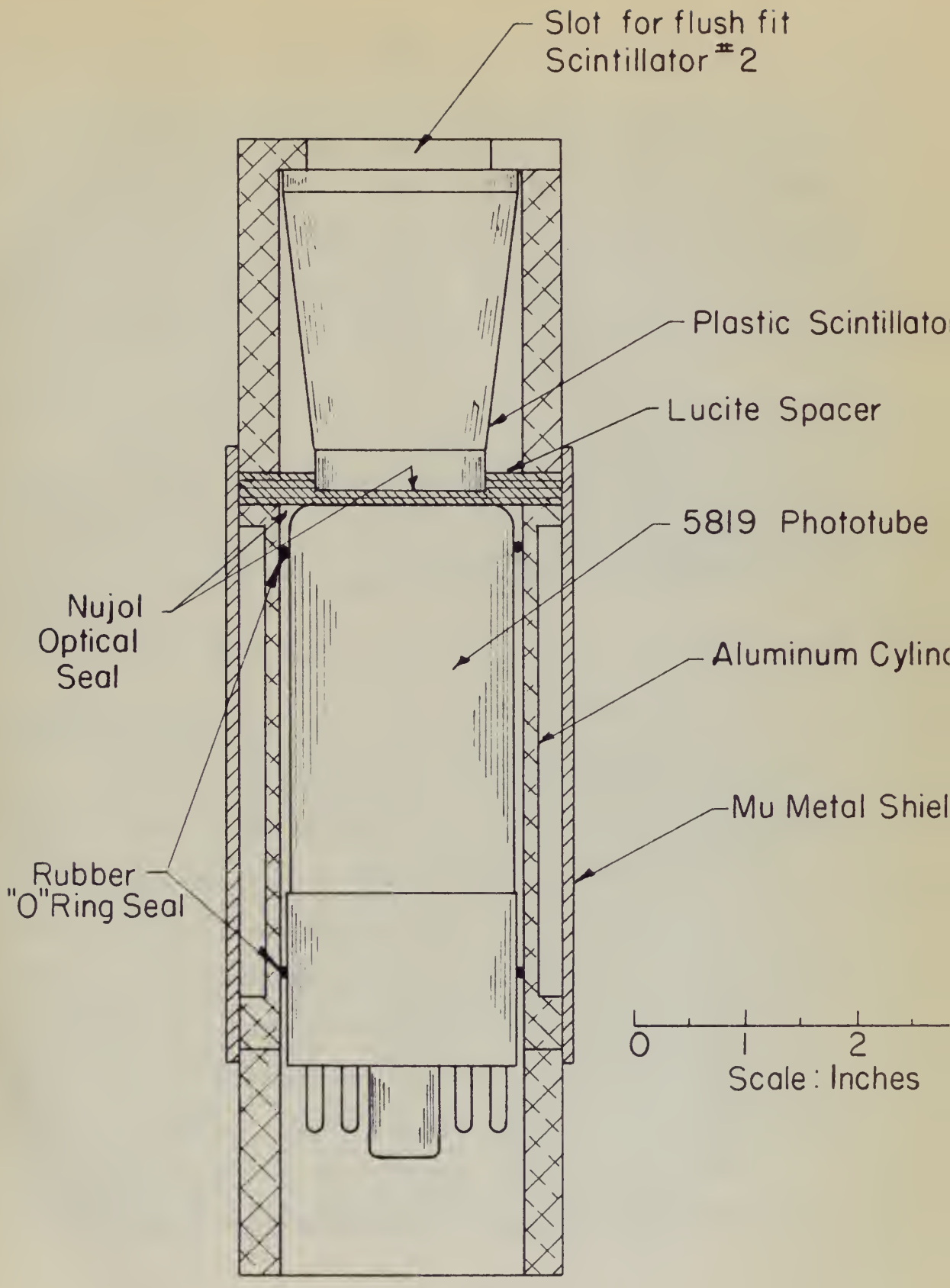

SCINTILLATION UNIT #1

Scintillator unit No. 2 has a 1-1/2 inch diameter, 2 inch long lucite light pipe, to which is screwed the 2-1/2 inch lucite light pipe shown in Figure 2. Scintillator No. 2 is inserted in the light pipe (push fit, Nujol optical seal). The converter holder fits into a larger diameter, 1/4 inch thick lucite ring which clamps unit No. 1 and unit No. 2 together.

Scintillator No. 3 is 1/8 inch by 1-1/8 inch, rectangular cross section, 2 inches long (shown in Figure 2). This domino-shaped plastic scintillator is held by a lucite clamp so that the standard 1-1/2 inch diameter lucite light pipe (as described for scintillator No. 2) looks at it end on.

ELECTRONIC CIRCUIT

The experimental equipment is shown in the block diagram of Figure 4. The gain of the system is calibrated by introducing artificial pulses (employing a Western Electric 275B relay to develop pulses of proper shape) into the input of the preamplifier. The height of these pulses is measured to an accuracy of a few tenths of a percent. The preamplifier is physically located as an integral part of the scintillation unit, bolted to the end of the aluminum housing of Figure 3. Pulses are then amplified times 30 in an amplifier whose rise time is 0.04 μ second. Unit No. 1 and unit No. 2 have two outputs. One output goes to the coincidence circuit and

Calorimeter unit No. 2 has a 1-1/2 inch diameter, 2 inch long Invite light pipe, to which is screwed the 2-1/2 inch Invite light pipe shown in Figure 3. Calorimeter No. 2 is inserted in the light pipe (unit #18, Type 1 optical seal). The converter holder fits into a larger diameter, 1/8 inch thick Invite ring which clamps unit No. 1 and unit No. 2 together.

Calorimeter No. 3 is 1/8 inch by 1-1/8 inch, rectangular cross section, 2 inches long (shown in Figure 2). This doming-shaped plastic calorimeter is held by a Invite clamp so that the standard 1-1/2 inch diameter Invite light pipe (as described for calorimeter No. 2) looks at it end on.

Electronic circuitry

The experimental equipment is shown in the block diagram of Figure 5. The path of the system is calibrated by introducing artificial pulses (employing a Hewlett Electric 27C11 relay to develop pulses of proper shape) into the input of the preamplifier. The height of these pulses is measured to an accuracy of a few tenths of a percent. The preamplifier is physically located as an integral part of the calorimeter unit, behind to the end of the aluminum housing of Figure 3. Pulses are then amplified times 30 in an amplifier whose rise time is 0.05 μ second. Unit No. 1 and unit No. 2 have two outputs. One output goes to the coincidence circuit and

the other to the addition circuit. The coincidence outputs from unit No. 1 and unit No. 2 are delay-line clipped to 0.05 μ second and delayed by 0.03 μ second to allow time for anticoincidence pulse No. 3 to function. These pulses are amplified and fed into an EFP 60-pulse shaper. The function of D2 is to discriminate against the Compton recoil electrons. D1 allows the biasing out of low-energy photons if desired. The output of EFP 60 No. 3 goes to the grid of the No. 2 Philips tube. Since the two inputs of the No. 2 EFP 60 are out of phase, if a signal exists at No. 3, there is no output from No. 2. The outputs of the No.1 and No. 2 pulse shapers to go a diode bridge.

The measurement of the resolving time of the spectrometer was experimentally determined, using the 6-Mev fluorine gamma-ray, to be 0.057 μ second, as shown in Figure 5. A DuMont 6292 phototube was tried in unit No. 1 but proved to be unsatisfactory. The fluctuations in the transit time for the DuMont tube were so large that the cable curve was not flat on top.

The other outputs from the No. 1 and No. 2 (x 30) amplifiers are added, clipped to 0.08 μ second, stretched, and amplified as shown by the block diagram of Figure 6. The output from the diode-bridge coincidence circuit triggers a univibrator which forms a 10 μ second gate. If the gate is open, the added pulse gets through and is amplified and then is pulse height analyzed.

Figure 4

Block Diagram of Experimental Equipment

The addition and gating circuit is shown in Figure 6, the pulse-height analysis circuit in Figure 7.

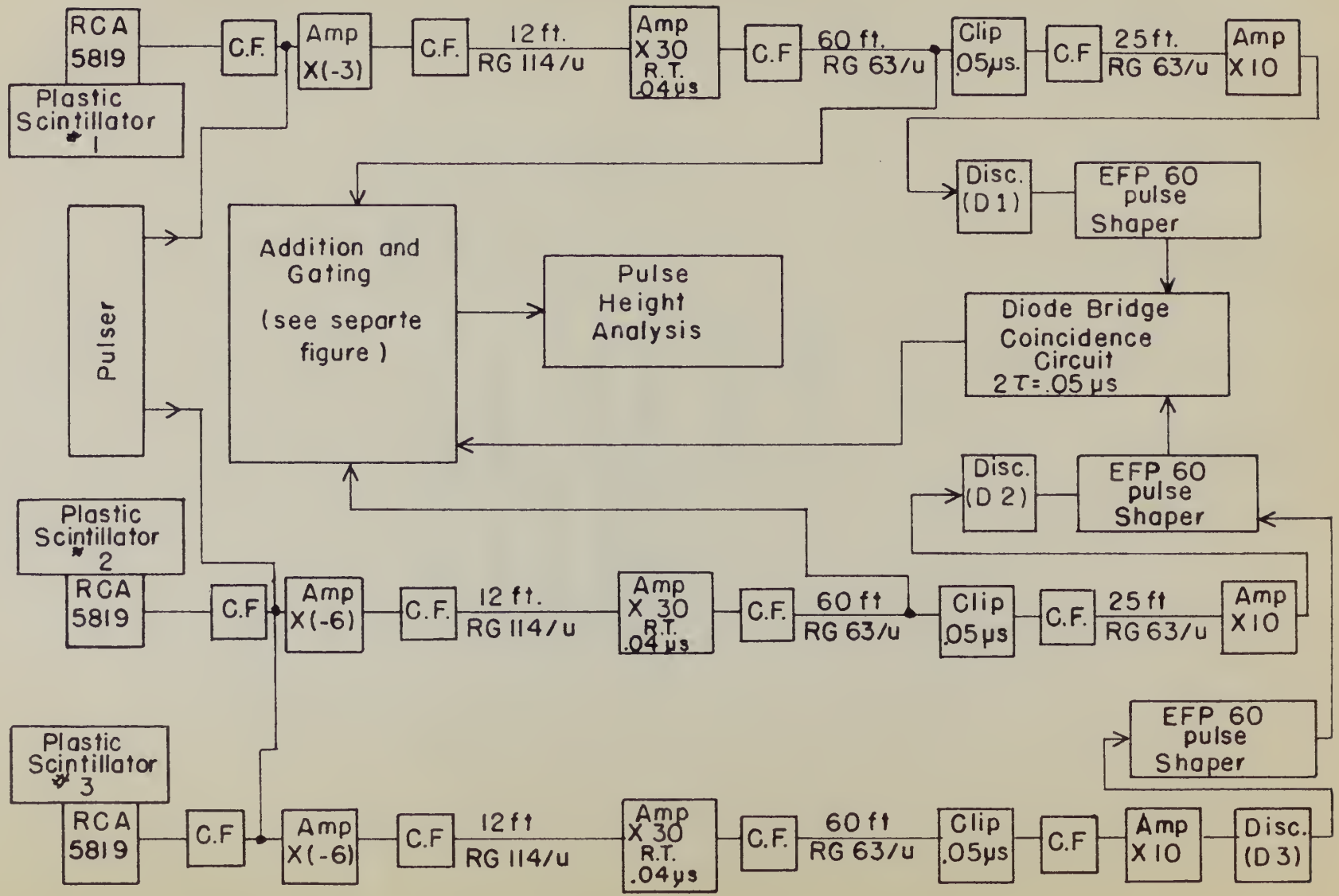

BLOCK DIAGRAM OF EXPERIMENTAL EQUIPMENT

Figure 5

Cable Curve

RG 63/U was used in conjunction with a $F^{19}(p,\alpha'\gamma)$ source to determine experimentally the resolivng time of the spectrometer. Each run was normalized to the same number of protons incident on the proton target.

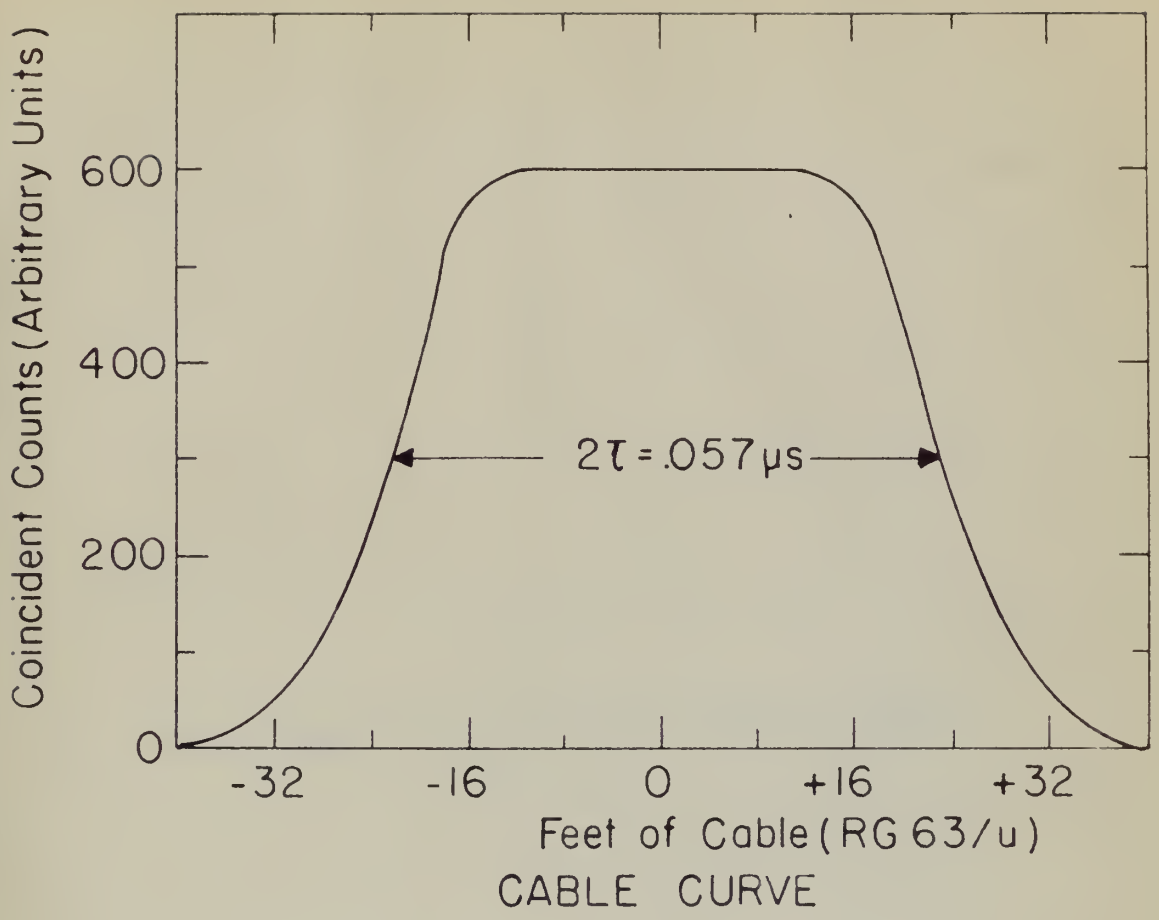
Coincident Counts (Arbitrary Units)
600
400
200
0
2τ = .057 μs
-32
-16
0
+16
+32
Feet of Cable (RG 63/u)

CABLE CURVE

Figure 6

Block Diagram of the Addition and Gating Circuit.

Figure 6

Blood Pressure of the Rabbits and Resting Circuit.

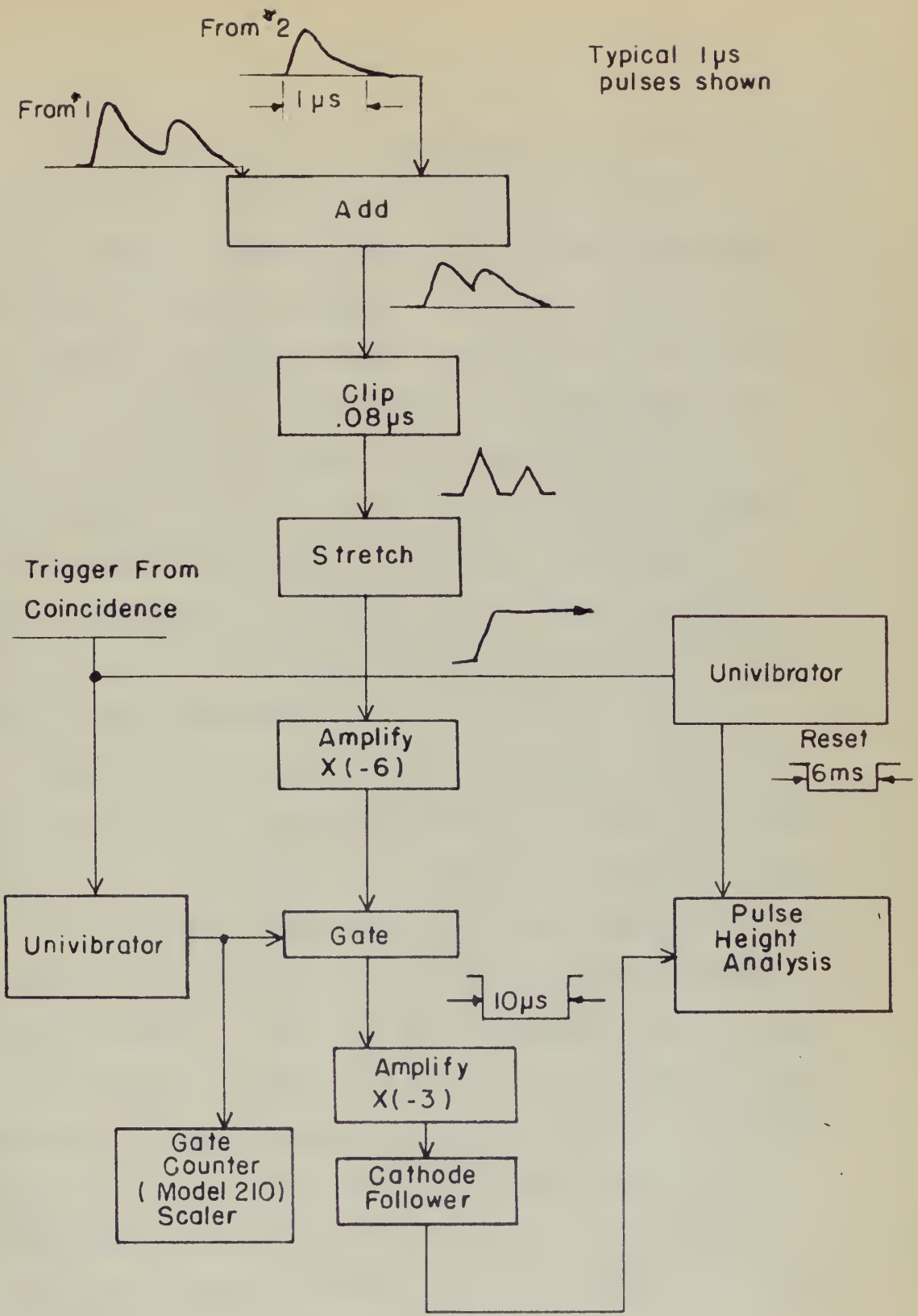

ADDITION AND GATING CIRCUIT

The pulse-height analysis circuit-block diagram is given in Figure 7. The basic principle of this pulse-height analysis is that pulse height is changed to time by a condenser discharging at constant current through a pentode. This time is accurately measured by beating a crystal-controlled oscillator on the triangular pulse and counting the oscillator pulses by a conventional binary scaler. This circuit is known as the "Multichannel Differential Discriminator," and its detailed circuit diagram may be found on file 6432, Laboratory for Nuclear Science, M. I. T., Dwg. No. D-2231-A. The output of the scaler goes to a buffer amplifier and then to one of two (or both simultaneously) methods of recording the reading of the scaler.

Figure 8 shows one method of data recording. This method provides a 128-channel recording pulse-height analyzer. Six scaler lights are in a light-tight box where they are recorded by a standard 16-mm movie camera externally driven at approximately 9 inches per minute. The framing pawl of the camera is removed to achieve continuous movement of the film. This is necessary, since the film is "framed" even though the camera shutter has been removed and made inoperative. A clock is an added feature for future identification. The film is read most easily by scanning it on a standard 16-mm microfilm reader. The pulser is turned on periodically during a run for calibration purposes. Reading time varies from 150 - 400 counts per hour, depending on energy and counting rate.

The pulse-height analysis circuit-block diagram is given in Figure 7. The basic principle of this pulse-height analysis is that pulse height is changed to time by a condenser discharging at constant current through a pentode. This time is accurately measured by beating a crystal-controlled oscillator on the triangular pulse and counting the oscillator pulses by a conventional binary scaler. This circuit is known as the "Multichannel Differential Discriminator," and its detailed circuit diagram may be found on file 6L32, Laboratory for Nuclear Science, M. I. T., Dwg. No. D-22311-A. The output of the scaler goes to a buffer amplifier and then to one of two (or both simultaneously) methods of recording the reading of the scaler.

Figure 8 shows one method of data recording. This method provides a 12?-channel recording pulse-height analyzer. Six scaler lights are in a light-tight box where they are recorded by a standard 16-mm movie camera externally driven at approximately 9 inches per minute. The feeding reel of the camera is removed to achieve continuous movement of the film. This is necessary, since the film is "reused" even though the camera shutter has been removed and made inoperative. A clock is an added feature for future identification. The film is read most easily by scanning it on a standard 16-mm microfilm reader. The pulser is turned on periodically during a run for calibration purposes. Reading time varies from 150 - 400 counts per hour, depending on energy and counting rate.

Figure 7

Block Diagram of the Pulse-Height Analysis Circuit

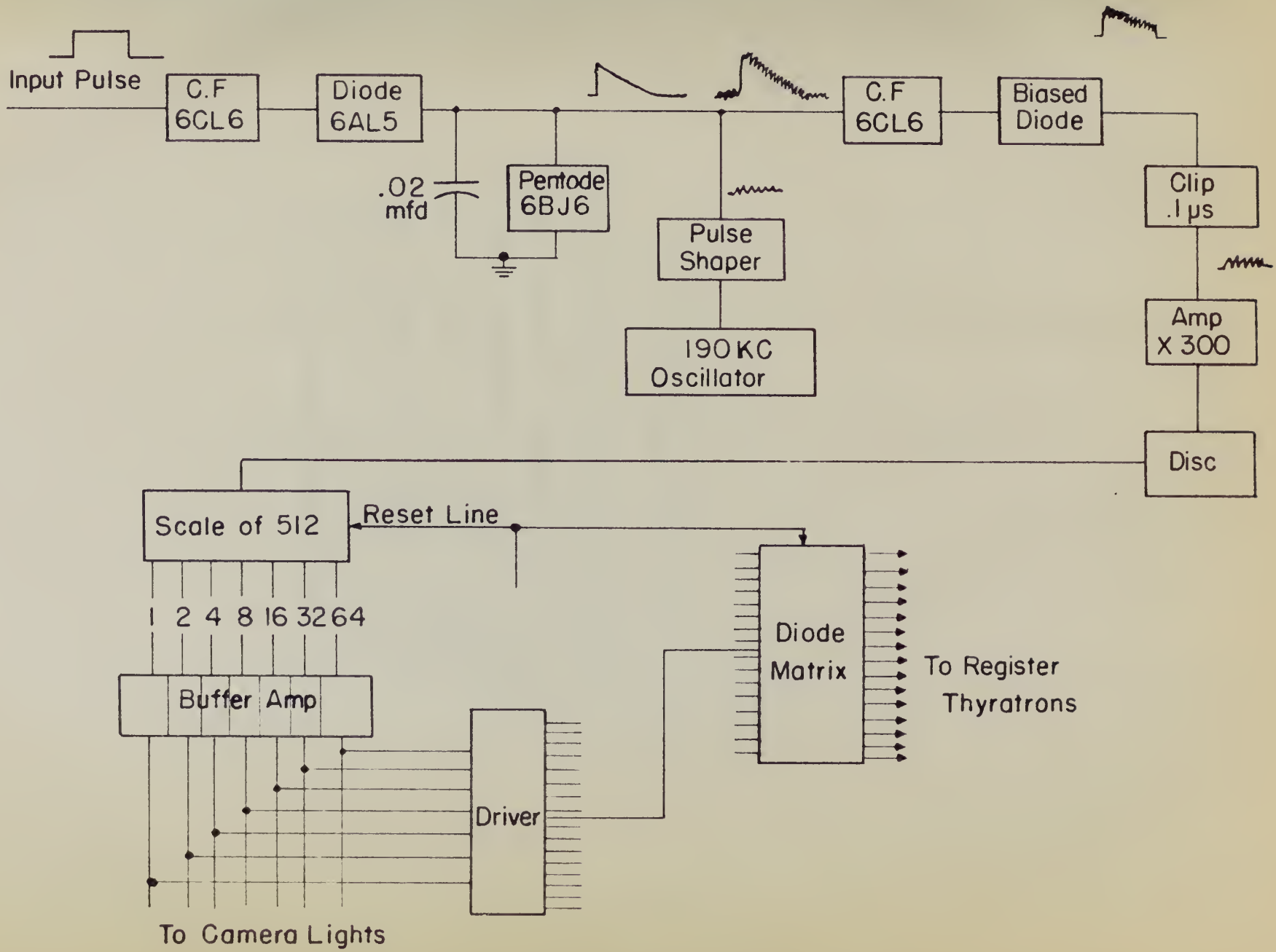

PULSE HEIGHT ANALYSIS CIRCUIT

Figure 8

Method of Recording Scaler Lights

The rectangular box shown in the figure is light-tight and a standard 16-mm movie camera, equipped with a short focal length lens, records the fact that the gate was opened and the channel number. The film is externally driven at 9 inches per minute. The clock is for identification of the run.

Figure 8

Method of Recording Scalar Lights

The rectangular box shown in the figure is
light-tight and a standard 16-mm movie
camera, equipped with a short focal length
lens, records the fact that the gate was
opened and the channel number. The film is
externally driven at 9 inches per minute.
The clock is for identification of the run.

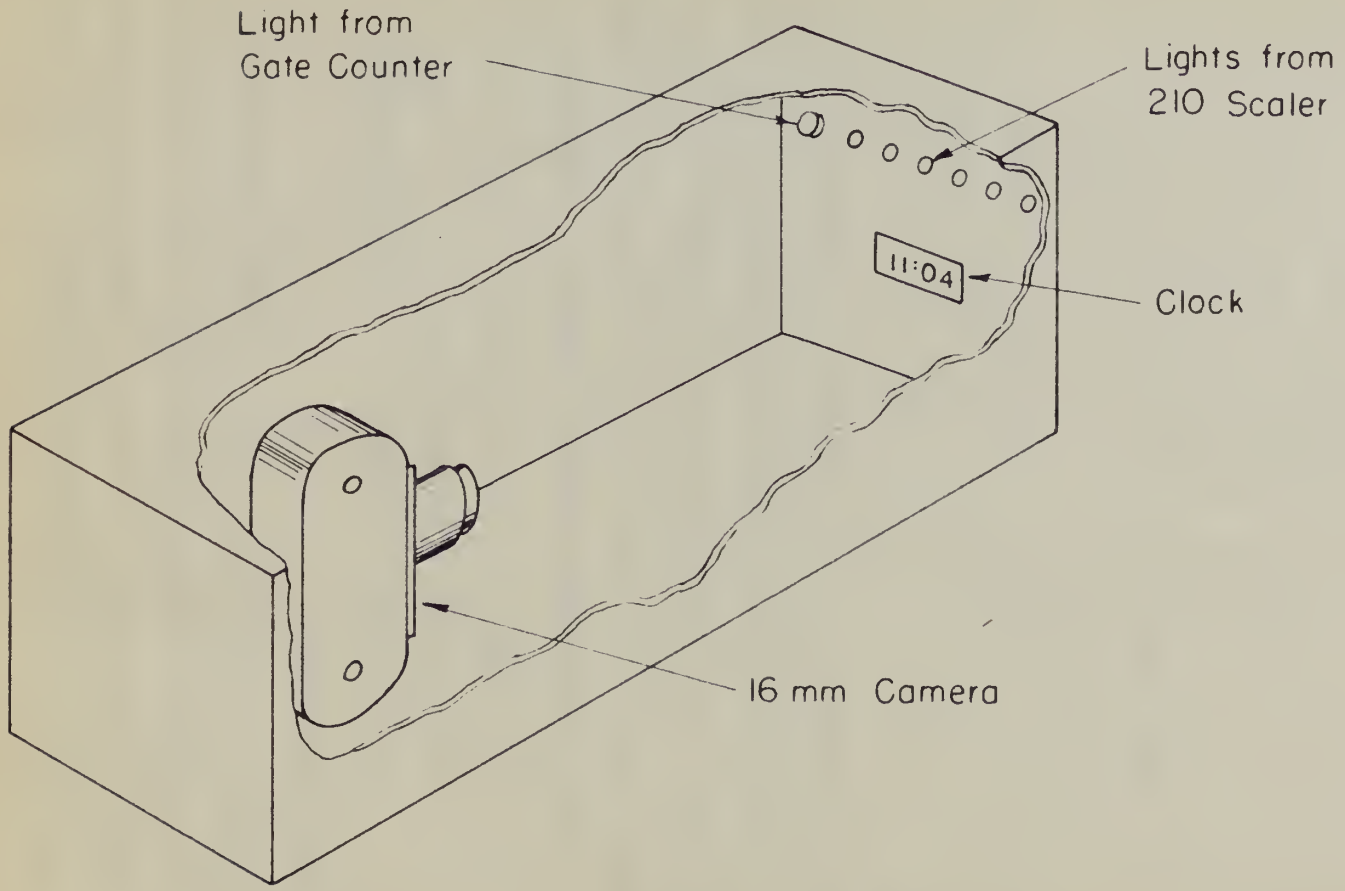
Light from
Gate Counter
Lights from
210 Scaler
11:04
Clock
16 mm Camera

The second method of recording the output of the analyzer is on a set of sixteen mercury registers. Essentially, the binary system of the scaler lights is converted into a scale of sixteen by means of a diode matrix. The sixteen registers can be set (by selector switch) to cover:

a. Channels 0-15, 16-31, 32-47, ..., 112-127;

b. Channels 0-31, 32-64, etc; or

c. Channels 0-63 and 64-127.

Investigation of the overall electronic stability of the spectrometer has shown a drift of the order of 1 percent during a period of one hour. It has been determined that the major part of the drift originates in the addition circuit. The pulse-height analyzer itself is stable to 1 percent over a period of several hours.

The second method of recording the output of the analyzer is on a set of sixteen memory registers. Essentially, the binary system of the scaler lights is converted into a scale of sixteen by means of a diode matrix. The sixteen registers can be set (by selector switch) to cover:

a. Channels 0-15, 16-31, 32-47, ..., 112-127;

b. Channels 0-31, 32-63, etc; or

c. Channels 0-63 and 64-127.

Investigation of the overall electronic stability of the spectrometer has shown a drift of the order of 1 percent during a period of one hour. It has been determined that the major part of the drift originates in the addition circuit. The pulse-height analyzer itself is stable to 1 percent over a period of several hours.

III. SELECTION OF PAIRS

The principle of selection of pairs created in the converter and rejection of Compton recoil electrons is accomplished by a discriminator in the output of unit No. 2 (D2 of Figure 4). Pairs are mostly emitted in the forward direction with the mean angle of bipartition given to a close approximation[21] by $\phi_0 = mc^2/E_p$, where mc^2 = 0.51 Mev, and E_p = photon energy less 1.02 Mev. The collision energy loss per cm for 1- to 15-Mev electrons is constant within 10 percent if the density effect[23] is included. Hence, to a first approximation, a pair will lose twice as much energy in scintillator No. 2 as will a Compton recoil electron. Therefore, we require that a minimum energy loss be sustained in scintillator No. 2 in order to record a coincidence with scintillator No. 1, resulting in addition of the energy lost by collision in Nos. 1 and 2, and yielding a pulse whose height is linearly proportional to the energy of the incident photon less 1.02 Mev.

For 17-Mev incident x-rays one would expect that D2 would do a good job of separating out the pairs. Figure 9 is an estimate of the pulse-height distribution for the 17.6-Mev incident gamma. Appendix I describes the method of obtaining this figure. One need only set D2 at 1.15-Mev energy loss in order to insure adequate pair selection.

III. SELECTION OF PAIRS

The selection of pairing of pairs created in the converter and detection of Cherenkov recoil electrons is accomplished by a discriminator in the output of unit No. 2 (U2 of Figure 6). Pairs are nearly emitted in the forward direction with zero angle of divergence since in a close approximation[21] $\sin\theta_0 = mc^2/E_\gamma$, where mc^2 = 0.51 Mev, and E_γ = photon energy above 1.02 Mev. The coincidence energy loss per cm for 1- to 17-Mev electrons in copper is 10 percent of the density effect[23] is included. Hence, in a first approximation, a pair will lose twice as much energy in penetrating 1cm. 2 cm will a Compton recoil electron. Therefore, we require that a minimum energy loss be detected to identify E_γ. I remember to consider a coincidence with scintillator No. 1, resulting in addition of the energy lost by collision in Nos. 1 and 2, and yielding a pulse whose height is linearly proportional to the energy of the incident electron above 1.02 Mev.

The 17-Mev Cockcroft accelerator would exceed that U2 would do a good job of reproducing such the value. Figure 9 is an estimate of the pulse-height distribution for the 17.6-Mev incident gamma. Another I describes the method of obtaining this figure. The need only set U2 at 1.1-Mev energy loss in order to insure adequate pair selection.

Figure 9

Calculated Differential Energy Distribution Curves for Scintillator No. 2, 17.6 Mev, 16-mil Pb Converter

The method of calculation of the curves is explained in Appendix I. The contribution to the distribution by pairs and Compton recoil electrons formed in the scintillator itself has not been taken into account.

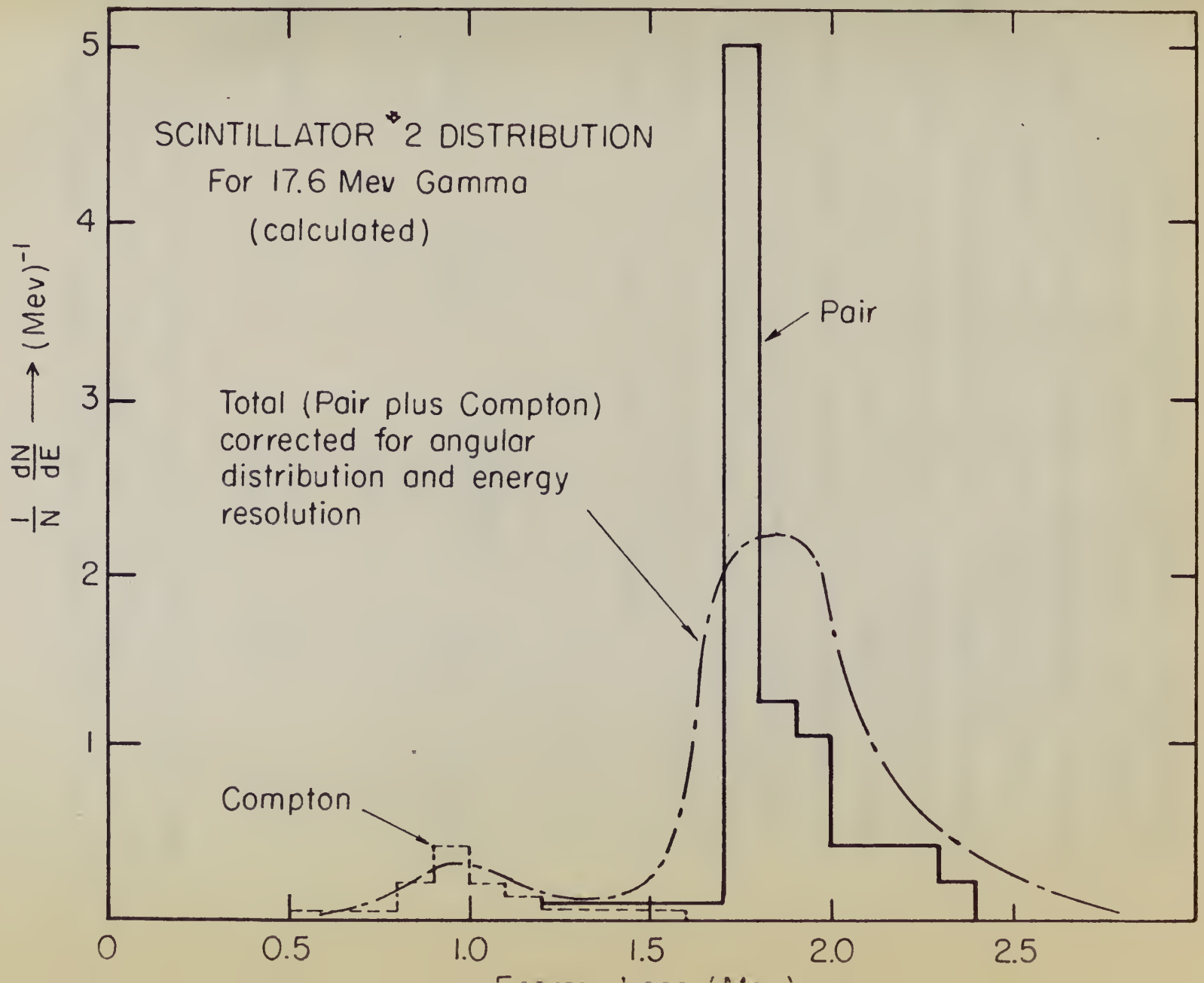
SCINTILLATOR #2 DISTRIBUTION
For 17.6 Mev Gamma
(calculated)
Pair
Total (Pair plus Compton)
corrected for angular
distribution and energy
resolution
Compton
$\frac{1}{N}\frac{dN}{dE} \longrightarrow (Mev)^{-1}$
5
4
3
2
1
0
0.5
1.0
1.5
2.0
2.5

At 6 Mev, a worthwhile estimate of the pulse-height distribution for scintillator No. 2 could only be obtained by a detailed "Monte Carlo"[14] calculation, which has not been carried out. It is more difficult to separate the pairs at 6 Mev than at 17 Mev.

Pairs and Compton recoil electrons may originate in scintillators themselves. If these electrons originate in scintillator No. 1, a coincidence will not be recorded. If they originate in the anti-coincidence unit, they will lose enough energy to trigger the anti-coincidence circuit and a coincidence count will not be recorded. However, if these electrons originate in scintillator No. 2, the possibility exists of recording a coincidence count. For comparison purposes, we examine the relative probabilities:

TABLE I

Process	16-mil Lead Converter	Scintillator No. 2	E_γ	Reference
Compton	0.7	0.9	6	25
Pair	1.0	0.1	6	14
Compton	0.32	0.39	17	25,29
Pair	2.1	0.25	17	29

Any pairs originating in unit No. 2, which lose enough energy in scintillator No. 2 to trigger D2, will contribute to a sharp resolution function. However, any Compton recoil electrons which are

Person	Half-wave limit (kv)	Retardation No. 2	$\bar{R}_T$	Reference
Compton	0.7	0.9	6	25
Tate	1.3	0.1	6	44
Compton	0.32	0.39	17	25,39
Tate	1.1	0.35	17	39

multiply scattered in scintillator No. 2 so as to trigger unit No. 2 (increased path length, increased energy loss by ionization) will result in the broadening of the shape of the spectrum, particularly on the low-energy side, because of the continuous Compton distribution. Qualitatively, it is seen that only low-energy Compton recoil electrons have a large probability of multiple scattering which, combined with their larger angle of emission (Appendix I), make this group the most troublesome. Hence, one way of cutting down the low-energy tail resulting from the Compton effect is to raise the bias of D1 or reduce the thickness of scintillator No. 2.

IV. FUNCTION OF SCINTILLATOR NO. 3.

Up to this point, it has been unnecessary to discuss scintillator No. 3 as the operation of the spectrometer as designed only requires unit No. 1 and unit No. 2, as previously described. At the near surface of scintillator No. 2, there may exist a high-level electron background. Most of these electrons come from the collimator.

For a 17-Mev incident gamma-ray, this large number of scattered electrons is an order of magnitude larger than the number created purposely in the converter. Some of these electrons will lose a sufficient amount of energy in scintillator No. 2 to contribute to the coincidence counting rate.

One can get rid of these electrons either by a magnet or by a third scintillator in anticoincidence. The setting of the discriminator on unit No. 3 is not critical. D3 is set so that a minimum ionizing particle in passing straight through scintillator No. 3 causes the anticoincidence circuit to operate.

V. RESOLUTION

Ideally, a monochromatic 5- to 17-Mev x-ray will interact with the converter forming pairs and Compton recoil electrons. As previously discussed, scintillation unit No. 2 will discriminate against the Compton recoil electrons, and pairs only will be recorded as coincidence counts, resulting in a single pulse height corresponding to $E_\gamma - 1.02$, where E_γ is incident monoenergetic x-ray energy in Mev. Resolution is defined as the width in Mev at half maximum divided by the peak energy in Mev.

The resolution of this spectrometer is determined by the following factors:

1. Light collection and photomultiplier statistics;
2. Radiation energy loss in the scintillators;
3. Electron escape from the scintillators;
4. Energy loss in the converter;
5. Capture of one or both annihilation quanta.

LIGHT COLLECTION AND PHOTOMULTIPLIER STATISTICS

The absorption of light is small[17] in plastic scintillators, such as "Pilot B." Photomultiplier statistics can be treated in good approximation[10,31,32] as a statistical fluctuation in the number of photoelectrons at the first dynode of the photomultiplier.

7. CONCLUSION

Ideally, a monochromatic 5- to 17-kev x-ray will interact with the converter through photo and Compton recoil electrons. As previously discussed, ionization with Be, Z will discriminate against the Compton recoil electrons, and pulse only will be recorded as coincidence events, resulting in a single pulse height corresponding to $E_\gamma - 3.5$, where E_γ is incident monochromatic x-ray energy in kev. Resolution is defined as the width in kev at half maximum divided by the peak energy in kev.

The resolution of this spectrometer is determined by the following factors:

1. Light collection and photomultiplier statistics;
2. Ionization energy loss in the scintillators;
3. Electron escape from the scintillators;
4. Energy loss in the converter;
5. Capture of one or both annihilation quanta.

LIGHT COLLECTION AND
PHOTOMULTIPLIER REACTION

The absorption of light in small[17] in plastic scintillators, such as "Pilot B." Photomultiplier statistics can be treated in good approximation[10,11,12] as a statistical fluctuation in the number of photoelectrons at the first dynode of the photomultiplier.

Mark and Goldring[13] have measured the resolution of the Cs^{137} 624-kev internal conversion line, using "Pilot B" scintillator and have obtained a value of 15 percent, as compared with 7 percent for NaI. This result implies an average of about 60 photoelectrons per Mev energy loss in the scintillator.

Using this figure of 60 photoelectrons per Mev energy loss and assuming that the light collection efficiency for scintillator No. 2 is half that for scintillator No. 1, we arrive at the following contributions to the energy resolution of the spectrometer resulting from light collection and photomultiplier statistics:

E_γ	Resolution (Percent.)
6	14
10	10
17	7

RADIATION ENERGY LOSS

Electron energy loss by radiation does not contribute to scintillator fluorescence. Bethe and Heitler[34] give the probability, P_α, that an electron traversing t radiation lengths will have an energy loss less than α times its initial energy (neglecting loss by ionization) as:

$$P_\alpha = \frac{\alpha^{t/\log 2}}{(t/\log 2)!},$$

Bark and Gridley[13] have measured the resolution of the Cs^{137} 631-kev internal conversion line, using "Pilot B" scintillator and have obtained a value of 12 percent, as compared with 7 percent for NaI. This result implies an average of about 60 photoelectrons per kev energy loss in the scintillator.

Using this figure of 60 photoelectrons per kev energy loss and assuming that the light collection efficiency for scintillator No. 2 is half that for scintillator No. 1, we arrive at the following contributions to the energy resolution of the spectrometer resulting from light collection and photomultiplier statistics:

E_γ	Resolution (Percent.)
6	18
10	10
17	7

RADIATION ENERGY LOSS

Electron energy loss by radiation does not contribute to scintillator fluctuations. Evans and Mettler[34] give the probability, P_a, that an electron traversing a radiation length will have an energy loss less than ϵ times the initial energy (neglecting loss by ionization) as:

$$P_a = \frac{\epsilon^{a}\sqrt{\log \tfrac{1}{\epsilon}}}{(a!)\sqrt{\log 2}} ,$$

where t is the thickness in radiation lengths[27]. A plot of this function for a 10-Mev electron traversing its total range is shown in Figure 10. If ionization losses and variation of the radiative loss with energy are taken into account[35], the effect will be to decrease further the low-energy tail. Examination of the energy distribution of the pairs[9,15] reveals that the low-energy tail will be further decreased; and, consequently, radiative loss at 17-Mev incident x-ray energy will not appreciably affect the resolution. Pairs from a 6-Mev incident x-ray will have negligible loss by radiation.

ELECTRON ESCAPE

Some of the electrons and positrons may escape from the scintillator. In calculating electron escape probability, the electron or positron was assumed to enter scintillator No. 2 at an average angle θ_0 (see Appendix I). The gaussian approximation of Rossi and Greisen[27] for the lateral displacement was graphically integrated taking into account the energy loss by collision. The mean square angle of scattering in the gaussian approximation[27] is:

$$\frac{Es^2t}{2\ p^2\beta^2},$$

where the meaning of the symbols is given in Appendix I. Thus, we find that a 15-Mev electron has an 18 percent probability of escaping with more than 1.5 Mev. Weighting the escape probability with

$$\frac{\mathrm{d}\sigma_{\mathrm{e}}}{\mathrm{d}\,\Omega_{\mathrm{e}}}$$

Figure 10

Electron Energy Loss by Radiation

This curve is the differential probability of energy loss by radiation for 100 10-Mev electrons traversing 0.15 radiation lengths in carbon.

Figure 10

Electron Energy Loss by Radiation

Data curve is the differential probability
of energy loss by radiation for 100 10-kev
electrons traversing 0.15 radiation lengths
in carbon.

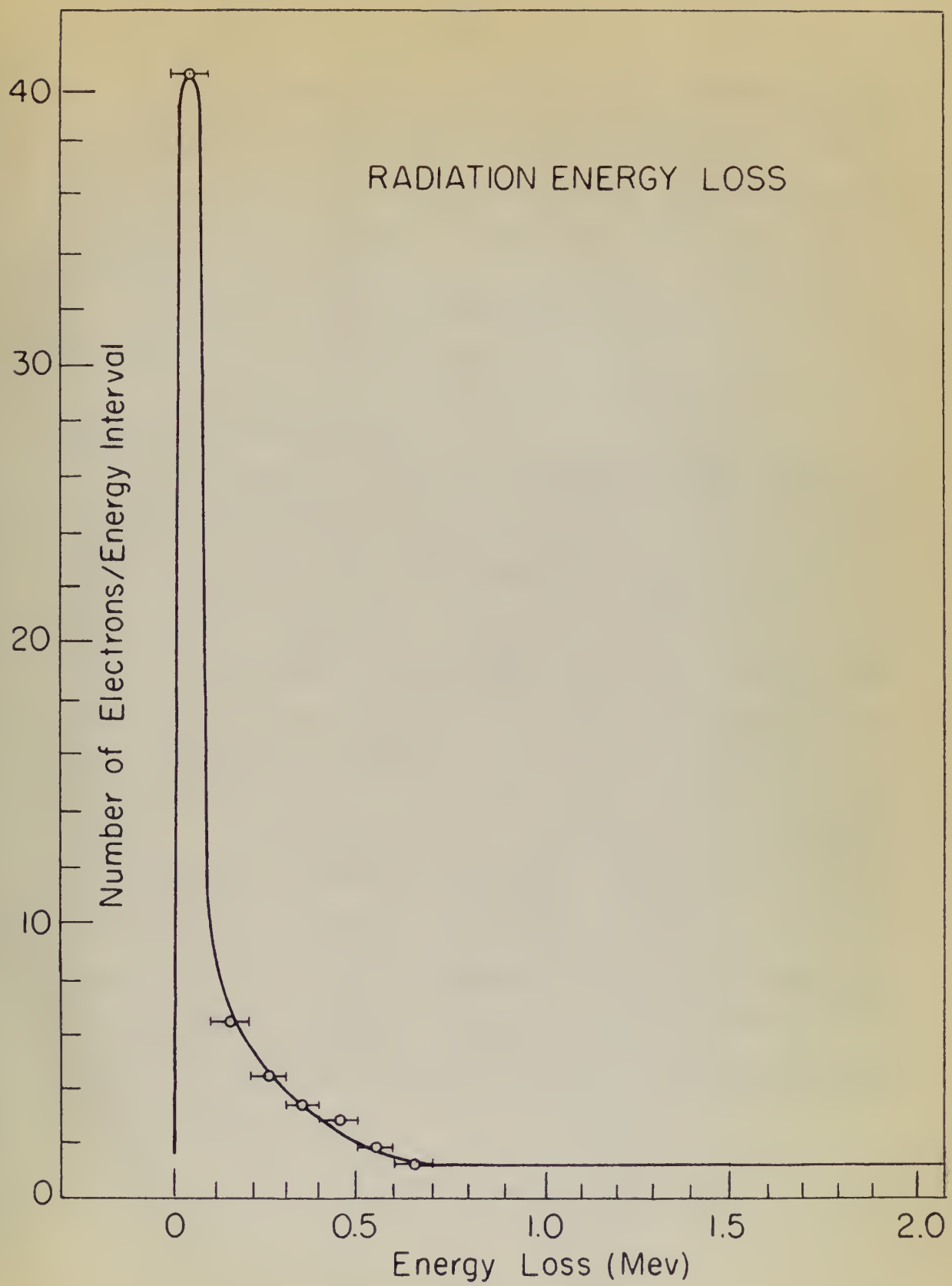
RADIATION ENERGY LOSS
Number of Electrons/Energy Interval
40
30
20
10
0
0
0.5
1.0
1.5
2.0
Energy Loss (Mev)

the pair energy distribution function[24] gives the approximate resolution caused by electron escape. This is negligible for a 5-Mev x-ray, of the order of 6 percent for the 17-Mev incident x-ray, and a rapidly increasing function of energy above 15-Mev x-ray energy. The length of scintillator No. 1 is equal to the range[36] of a 16-Mev electron.

ENERGY LOSS IN THE CONVERTER

The electron pair created in the converter loses energy in the converter and in the aluminum foil before entering the scintillator. This energy loss is not a constant, and the fluctuations in this energy loss contribute to the energy resolution of the spectrometer. The fluctuation of energy loss occurring when electrons pass through absorbers that are thin compared with their range has been experimentally measured[37-39] and found to agree with the Landau theory[40]. The net effect of multiple scattering is to increase the relative number of low-energy electrons[28]. The rms fluctuation in energy loss can be most easily calculated using Yang's Δ correction and assuming the gaussian distribution for the multiple scattering (see Appendix I). Proceeding along these lines, we calculate a root mean square energy loss, which, when divided by the electron energy, gives resolution.

the pair energy distribution function[21] gives the approximate relation between $\bar{\epsilon}$ and ϵ. This is negligible for a 5-Mev x-ray, or the number of 6 percent for the 17-Mev incident x-ray, and a rapidly increasing function of energy above 15-Mev x-ray energy. The length of retardiator R_0, I is equal to the range[36] of a 16-Mev electron.

ENERGY LOSS IN THE CONVERTER

The electron pair created in the converter loses energy in the converter and in the climbing foil before entering the ionization. This energy loss is not a constant, and the fluctuations in this energy loss contribute to the energy resolution of the spectrometer. The fluctuation of energy loss occurring when electrons pass through absorbers that are thick compared with their range has been experimentally measured[37-39] and found to agree with the Landau theory[40]. The net effect of multiple scattering is to increase the relative position of low-energy electrons[23]. The rms fluctuation in energy loss can be most easily calculated using Fano's[3] correction and combining the Gaussian distribution for the multiple scattering (see Appendix I). Proceeding along these lines, we calculate a root mean square energy loss, $\sigma_{\Delta E}$, when divided by the electron energy, gives resolution.

The aluminum foil used to wrap the scintillator has a total thickness of 3 mils. At 6 Mev, the energy loss calculated as outlined above is of the order of 1 percent; at 17 Mev, this loss is negligible.

The converter can be approximated as an electron point source covered with a foil of half converter thickness. The angular distribution of the electrons in pair production will in general have the same effect as multiple scattering; that is, electrons will not travel a constant straight-line path through the foil but will be distributed in direction (hence, path length) according to the pair production angular distribution. Since a characteristic angle of emission (see Appendix I) is inversely proportional to energy, as also is the root mean square angle of scattering, the ratio of these two angles is roughly independent of energy for a given converter thickness. No gain in resolution can be achieved by reducing the converter thickness beyond the point where the root mean square scattering angle becomes equal to the average angle of pair emission.

Assuming an average electron energy equal to one-half $(E_\gamma - 1.02)$, where E_γ is incident x-ray energy in Mev, the following results are obtained for a 16-mil lead converter:

E_γ	Resolution (Percent.)
6	14
11	5.7
17	3.5

E_γ	Transition (forward.)
4	1b
13	5-1
17	3-S

The effect of radiation loss in the converter is smaller than the above.

CAPTURE OF ANNIHILATION QUANTA

Capture of an appreciable fraction of the annihilation quanta in the scintillator will impair the energy resolution of the spectrometer.

The fraction of gamma-ray energy dissipated by a narrow beam in passing through the scintillator is not the same as the fractional loss of intensity. It is necessary to multiply the probability of each interaction process (Compton and photoelectric) by the probable fraction of the photon energy actually dissipated in the absorber as a result of the process. Using this method, one takes the value of the energy absorption coefficient to be 0.029 cm^2/gm at 0.51 Mev for "Pilot B" scintillators (Fano[41]).

The method used to calculate the probability that at least one annihilation quantum is absorbed is as follows: Assume an average angle of pair emission and that the range of the electron[18] is approximately that for aluminum. (The energy loss in mica, carbon, and air is not significantly different from that in the same weight of aluminum[33].) From this stopping point, assuming the quanta are isotropically emitted back-to-back with equal energies[21], we establist an average solid angle and an average path length. From this

is calculated the average energy absorbed by the scintillator, taking into account the energy distribution function of the pair electrons. At 17 Mev, about 4 percent of the annihilation quanta are absorbed in the scintillator and about 7 percent are absorbed at 6 Mev.

SUMMARY OF EXPECTED RESOLUTION

To summarize this chapter, assuming that the processes above are statistically independent[22], one arrives at the following values for the expected resolution of the spectrometer when using a 16-mil lead converter:

E_γ	Resolution (Percent.)
6	20
10	12
17	10

is calculated the energy energy absorbed by the scintillator, taking into account the energy distribution function of the pair electrons. At 17 Mev, about 5 percent of the annihilation events are absorbed in the scintillator and about 7 percent are absorbed at 6 Mev.

SUMMARY OF EXPECTED RESOLUTION

To summarize this chapter, assuming that the processes above are statistically independent[22], one arrives at the following values for the expected resolution of the spectrometer when using a 16-cell lead converter:

E_γ	Resolution (Percent.)
6	30
10	12
17	10

VI. CALIBRATION AT THE ROCKEFELLER GENERATOR

The spectrometer is calibrated by using two gamma-rays of known energies to provide the two points necessary to draw the linear characteristics[9-11] of the scintillator. Since there are no available monoenergetic gamma sources about 5 Mev, it is necessary to utilize gamma-rays from nuclear reactions. The source of gamma-rays generally used for this type of work is from the proton bombardment of light elements.

The source of protons for testing the spectrometer was the M.I.T. Rockefeller electrostatic generator. This generator is capable of delivering a magnetically analyzed (to within 0.1 percent) proton beam of 5 microamperes, continuously variable from 0.7 to 4 Mev. The output proton current is determined by a proton beam current integrator. The area of the proton beam at the target is about 4 square millimeters, so that for the purposes of this experiment the gamma-ray originates from a point source. Figure 11 shows a photograph of the spectrometer and proton target. A scale drawing showing distances from the source is given in Figure 1.

In view of the difficulty of preparing thin proton targets that will physically withstand high proton bombardment current, it was decided to use thick targets. Targetholders were made of 10-mil aluminum disks 2 inches in diameter. A 1/16 inch deep 1/2 inch

VI. CALIBRATION AT THE BOOSTER/LINE INTERFACE

The spectrometer is calibrated by using two beam-type of known energies to provide the two points necessary to draw the linear characteristics[9-11] of the potentiometer. Since there are no available monoenergetic beams accurate about 5 Mev, it is necessary to utilize beam-types from nuclear reactions. The reaction of beam-type generally used for this type of work is from the proton bombardment of Lithium Fluoride.

The energies of protons for meeting the spectrometer was the M.I.T. Cambridge electrostatic generator. This generator is capable of delivering a magnetically analyzed (to within 0.1 percent) proton beam of 5 micro-amperes, continuously variable from 0.7 to 5 Mev. The output proton current is determined by a proton beam current integrator. The area of the proton beam at the target is about 1 square centimeter, so that for the purposes of this experiment the beam-type originates from a point source. Figure 11 shows a photograph of the spectrometer and proton target. A scale drawing showing distances from the source is given in Figure 1.

In view of the difficulty of penetrating thin proton barriers that will operate with extended high proton bombardment current, it was decided to use thick targets. Targets/films were made of 10-mil aluminum disks 2 inches in diameter. A 1/16 inch deep 1/2 inch

Figure 11

The Spectrometer in Place at the MIT Rockefeller Generator

This figure is a photograph of the spectrometer at the Rockefeller generator as it was located for testing and calibration. The proton target is shown in the right of the photograph.

Figure 13

The Spectrometer in Case at the ATI Exploratory Conference

This figure is a photograph of the spectrometer at the Exploratory conference as it was located for testing and calibration. The various ranges in views is the photometric rights of the photometric.

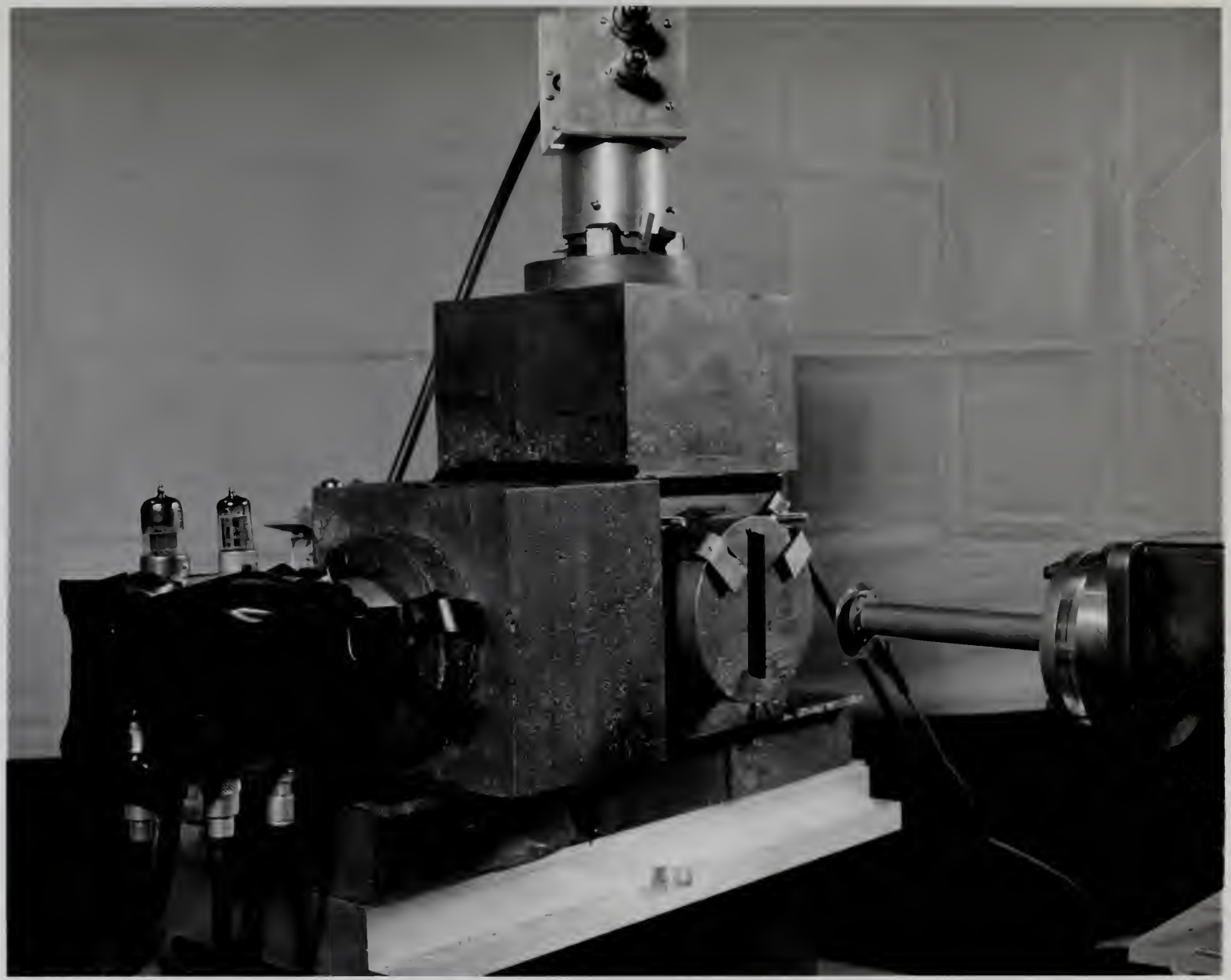

diameter recess was formed in the center of the aluminum disk to hold the target material. Using the same die used to make the depression, the target material was pressed into the recess. This method proved satisfactory for all materials other than boron. The B_4C sample was obtained through the courtesy of Professor J. T. Norton, Metallurgical Department, M. I. T. It was in the form of a 3/16 inch thick sample, hot pressed in a graphite die.

A list of energy standards used and references giving the yields and gamma-ray energies follows:

TABLE II

Target Material	Proton Bombardment Energy (Mev)	Gamma Energy (Mev)	Yield ($\gamma/10^9$ Protons)	Reference
B_4C	1.2	16.7	2	12
		12.12	4	12
		4.41	4	12
CaF	1.15	6.13	500	4,12
		7.0	200	4,12
Li Metal	1.15	17.6	20	4,16
		14.8	30	4,16

To a first approximation, the counting rate of the spectrometer is the fraction of solid angle subtended times the probability

diameter recess was formed in the center of the aluminum disk to hold the target material. During the runs dia used to make the depression, the target material was pressed into the recess. This method proved satisfactory for all materials other than boron. The B_4^C sample was obtained through the courtesy of Professor J. T. Norton, Metallurgical Department, M. I. T. It was in the form of a 3/16 inch thick sample, not pressed in a graphite die.

A list of energy standards used and references giving the yields and gamma-ray energies follows:

TABLE II

Target Material	Proton Bombarding Energy (Mev)	Gamma Ray Energy (Mev)	Yield (γ/10^9 Protons)	Reference
B_4^C	1.2	16.7	2	12
		12.12	4	12
		4.41	4	12
C$_{nf}$	1.15	6.13	500	4.12
		7.0	800	4.12
Li Metal	1.15	17.6	30	4.16
		14.8	30	4.16

To a first approximation, the counting rate of the spectrometer is the fraction of solid angle subtended times the probability

of producing a pair in the converter times the rate of emission of gamma radiation. The actual efficiency of the counter must be determined by experiment, since the efficiency is an unknown function of D2 and D1 settings, as well as the incident x-ray energy.

Taking into consideration target conditions, pair cross section, and solid angle which obtain at the Rockefeller generator, it was determined that the approximate times to record 1000 counts are as follows:

Target	Time
CaF	10 min
Li	1 hour
B_4C	1 hour

The danger of contaminating the Rockefeller generator imposes a proton current limitation when bombarding lithium targets; this limitation is not present with B_4C. This fact, coupled with the formation of LiOH at the surface, reduces the maximum attainable lithium yield by about a factor of 10, which effectively gives the same obtainable counting rate for lithium and boron.

of producing a pair in the converter times the rate of emission of gamma radiation. The actual efficiency of the converter must be determined by experiment, since the efficiency is an unknown fraction of 1% but it matters, as well as the Geiger x-ray energy.

Taking into consideration target conditions, pair yield, geometry, and solid angle which obtain at the Borderlite generator, it was determined that the approximate times to record 1000 counts are as follows:

Source	Time
Ra	10 min
Be	1 hour
D_2O	1 hour

The danger of contaminating the Borderlite generator imposes a proton current limitation when bombarding lithium targets; this limitation is not common with D_2O. This fact, coupled with the formation of LiOH at the surface, reduces the maximum attainable lithium yield by about a factor of 10, which effectively gives the same obtainable counting rate for lithium and beryl.

VII. DISCUSSION OF EXPERIMENTAL RESULTS

ENERGY CALIBRATION

The calibration of the spectrometer is in terms of the pulser voltage. The raw data are, however, recorded in terms of channel number. The channel number (C) is related to voltage by:

$$C = f(V_{1a} + K'V_{2a}) \qquad (1)$$

where V_{1a} and V_{2a} are input pulse heights in volts to the addition circuit from units Nos. 1 and 2, respectively; K' is an amplification factor determined by the parameters of the addition circuit. Assuming linearity as far as the addition circuit, equation (1) may be written:

$$C = g(V)$$

where $V = 3(V_1 + KV_2)$; V_1 and V_2 are the output voltage of scintillation units Nos. 1 and 2, respectively. V is a pulser voltage, and the factor of 3 comes from the parameters of the circuit in which pulser and photomultiplier signals are mixed.

A typical calibration curve, giving $C = g(V)$, is shown in Figure 12. The calibration curve is measured both with $V_2 = 0$ and $V_1 = V_2$ in order to determine the addition factor K. The value of K ordinarily used was 0.450 and was stable to 0.5 percent for several hours. The nonlinearity at the upper end of the curve shown in

VII. INTRODUCTION OF EXPERIMENTAL ERRORS

ENERGY CALIBRATION

The calibration of the spectrometer is in terms of the pulser voltage. The raw data are, however, recorded in terms of channel number. The channel number (U) is related to voltage by:

$$U = f(K V_{in} + K' V_{2n}) \qquad (1)$$

where V_{in} and V_{2n} are input pulse heights in volts to the addition circuit from units Nos. 1 and 2, respectively; K' is an amplification factor determined by the parameters of the addition circuit. Assuming linearity as for an addition circuit, equation (1) may be written:

$$U = f(V)$$

where $V = j(V_j + KV_2)$; V_j and V_2 are the output voltage of calculation units Nos. 1 and 2, respectively. V is a pulser voltage, and the factor of j comes from the parameters of the circuit in which pulser and photomultiplier signals are mixed.

A typical calibration curve, giving $U = f(V)$, is shown in Figure 12. The calibration curve is measured both with $V_2 = 0$ and $V_j = V_2$. In order to determine the addition factor K. The value of K ordinarily used was 0.250 and was stable to 0.5 percent for several hours. The nonlinearity at the upper end of the curve shown in

Figure 12

Calibration Curve

Shown here is a typical calibration curve made before, during, and after each run. Raw data are in the form of counts per channel as a function of channel number. Data are converted into counts per volt as a function of pulser voltage.

Figure 32

Dimensioning Curve

Shown here is a typical multimeshing curve
made before, during, and after wash run.
Time scale are in the form of examine one obser-
vation as a function of observed number. Index
are converted into counts per volt as a
function of primary voltage.

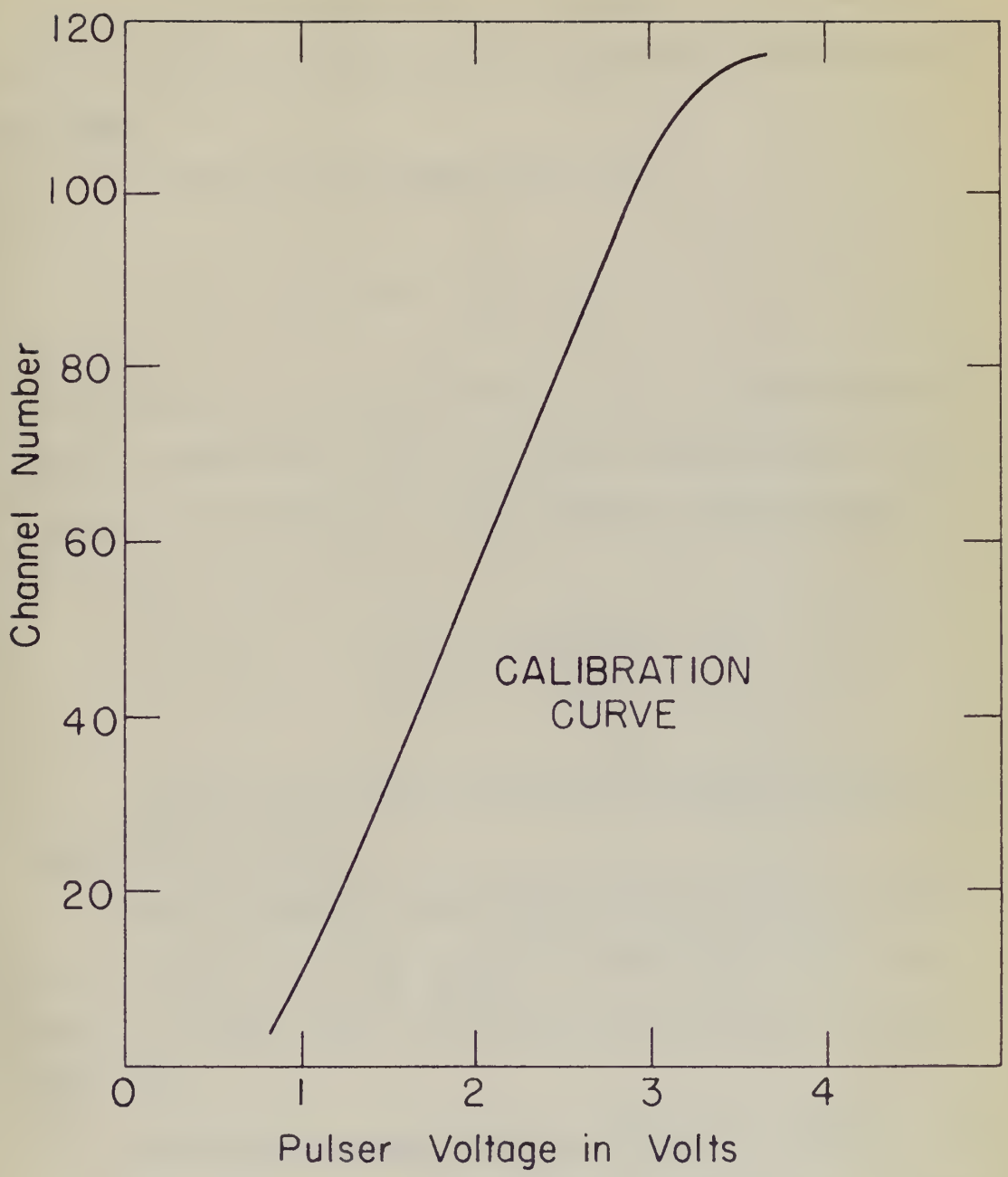
120
100
80
60
40
20
Channel Number
CALIBRATION
CURVE
0
1
2
3
4
Pulser Voltage in Volts

Figure 12 comes from overloading the stage of amplification just before the pulse-height analyzer. The nonlinearity in the lower part of the curve comes from diode nonlinearity in the pulse-height analyzer.

The energy of the incident x-ray is:

$$E_\gamma = 1.02 + E_1 + E_2 + E_c ,$$

where E_1 and E_2 are energy losses (in Mev) in scintillators Nos. 1 and 2, respectively, and E_c is the most probable energy lost by electrons and positrons in the lead converter (about 0.5 Mev).

$$V = \frac{V_1}{E_1} E_1 + K \frac{V_2}{E_2} E_2 .$$

The ratios V_1/E_1 may be controlled by varying the photomultiplier high voltage.

The same negative power supply furnished the high voltage for No. 1 and No. 2. This supply was stable to 0.1 percent for periods of several hours. Both photomultipliers were operated at -740 volts.

Calibration was accomplished by varying the addition factor, K, until the peaks from the 6-Mev fluorine line and the 16-Mev B_4C line fell in the correct relative positions (see Figure 13).

Figure 12 shows those unwanted the stage of amplification just before the pulse-height analyzer. The resolution in the lower part of the curve comes from clock resolution in the pulse-height analyzer.

The energy of the incident x-ray is:

$$E_\gamma = 1.02 + E_1 + E_2 + E_3 \text{ ,}$$

where E_1 and E_3 are energy losses (in Mev) in scintillators No. 1 and 3 respectively, and E_2 is the most probable energy lost by electrons and positrons in the lead converter (above 0.5 Mev).

$$\text{v} = \frac{\gamma_1}{\beta_1} E_1 + \varepsilon \frac{\gamma_2}{\beta_2} E_2.$$

The ratios γ_1/β_1 may be controlled by varying the photomultiplier high voltage.

The same regulated power supply furnished the high voltage for Nos. 1 and No. 2. This supply was stable to 0.1 percent for periods of several hours. Both photomultipliers were operated at -710 volts.

Calibration was accomplished by varying the addition factor, E_3, until the peaks from the 6-Mev fluorine line and the 16-Mev O^{16} line fell in the correct relative positions (see Figure 13).

Figure 13

Energy Calibration

Curve No. 1 was obtained by proton bombardment of a thick CaF target; curve No. 2 by proton bombardment of a thick B_4C target. A 16-mil lead converter was used for both curves. The boron curve (No. 2) from 1.5 - 2.5 volts was obtained with poor statistics and normalized to match the 2.5 - 4.5 volt section. There is some evidence of the 12-Mev line at 2.3 volts. The anticoincidence circuit had not been designed when these runs were made.

Figure 13

Energy Calibration

Curve No. 1 was obtained by proton bombardment of a thick BF_3 target; curve No. 2 by proton bombardment of a thick B_2^{11} target. A 16-cell ional chamber was used for both curves. The boron curve (No. 2) from 1.5 - 2.5 volts was obtained with poor statistics and interpolated to obtain the 2.6 - 4.7 volt section. There is some evidence of the 12-Mev line at 3.3 volts.

The multivibrator circuit had not been designed when these runs were made.

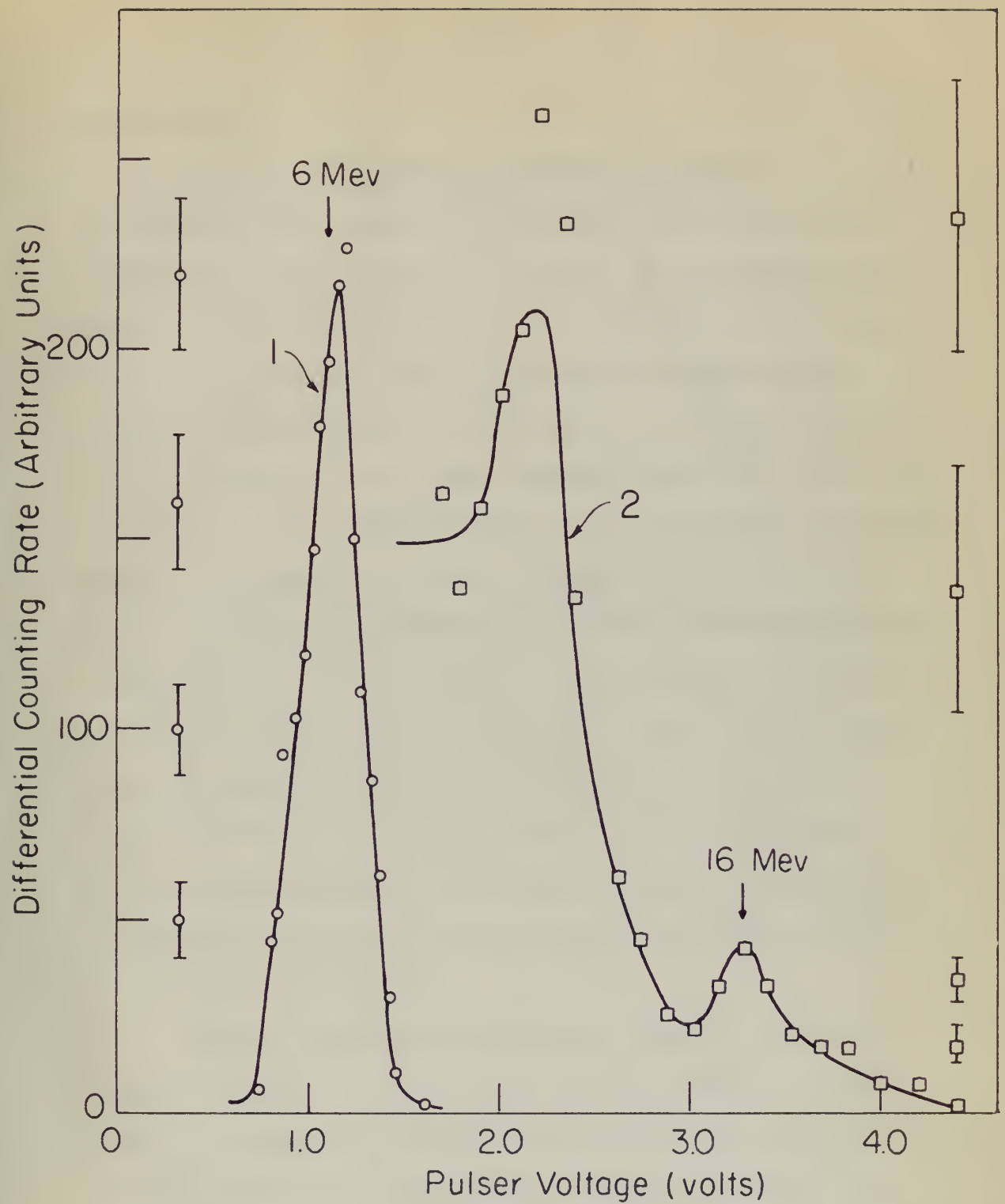
6 Mev
1
2
16 Mev
Differential Counting Rate (Arbitrary Units)
200
100
0
0
1.0
2.0
3.0
4.0
Pulser Voltage (volts)

FLUORINE RUNS

The low-energy limitation of the spectrometer is imposed by the rapid decrease of the pair production cross section with decreasing energy, combined with the increase in Compton cross section. At about 5 Mev (where these two cross sections are about equal), the resolution of the spectrometer is limited by the inability of discriminator No. 2 to perform its designed function; that is, separation of the doubly ionizing pulses of the pair process from the singly ionizing pulses of the Compton recoil electrons. Figure 14 illustrates the lack of a definite separation between pairs and Compton recoil electrons for 6-Mev incident x-ray energy. A sufficiently thin converter with a very thin scintillator No. 2 would perform this function at, say, 3 Mev, since multiple scattering in the converter and in the scintillator, with consequent increased fluctuations in the energy loss, would be minimized. A point is reached, however, where light collection difficulties and photomultiplier statistics impose a lower energy limit to the usefulness of the spectrometer.

Figure 15 illustrates the effect of changes in spectrum shape with changes in D1. In order for the spectrometer to function, it is necessary that there be a region where changing D1 does not materially affect spectrum shape. Figure 15 illustrates that such a plateau does in fact exist; that is, changing D1 from very

PLOTTING ITEMS

The low-energy limitation of the spectrometer is imposed by the rapid decrease of the pair production cross section with decreasing energy, combined with the increase in Compton cross sections. At about 5 Mev (where these two cross sections are about equal), the resolution of the spectrometer is limited by the inability of discriminator No. 2 to perform its designed function; that is, separation of the doubly ionizing pulses of the pair process from the singly ionizing pulses of the Compton recoil electrons. Figure 10 illustrates the lack of a definite separation between pairs and Compton recoil electrons for 6-Mev incident x-ray energy. A sufficiently thin converter with a very high scintillator No. 2 would perform this function at, say, 3 Mev, since multiple scattering in the converter and in the scintillator, with consequent increased fluctuations in the energy loss, would be minimized. A point is reached, however, where light collection difficulties and photomultiplier statistics impose a lower energy limit to the usefulness of the spectrometer.

Figure 11 illustrates the effect of changes in spectrum shape with changes in Ω. In order for the spectrometer to function, it is necessary that there be a region where changing Ω does not materially affect spectrum shape. Figure 12 illustrates that such a plateau does in fact exist; that is, changing Ω from very

Figure 14

Pulse-Height Distribution for Scintillator No. 2 at 6 Mev
This curve was obtained by the proton bombardment of a thick CaF target using a 16-mil lead converter. The standard statistical errors of the points are indicated to the right of the curve.

Figure 1A

Poly-Phiphi Distribution for Retail Stores No. 7 at 6 day
This curve was obtained by the proton bombardment
of a block for longer period a lined sloping
ken. The absolute statistical accuracy of the
values are indicated to the right of the curve.

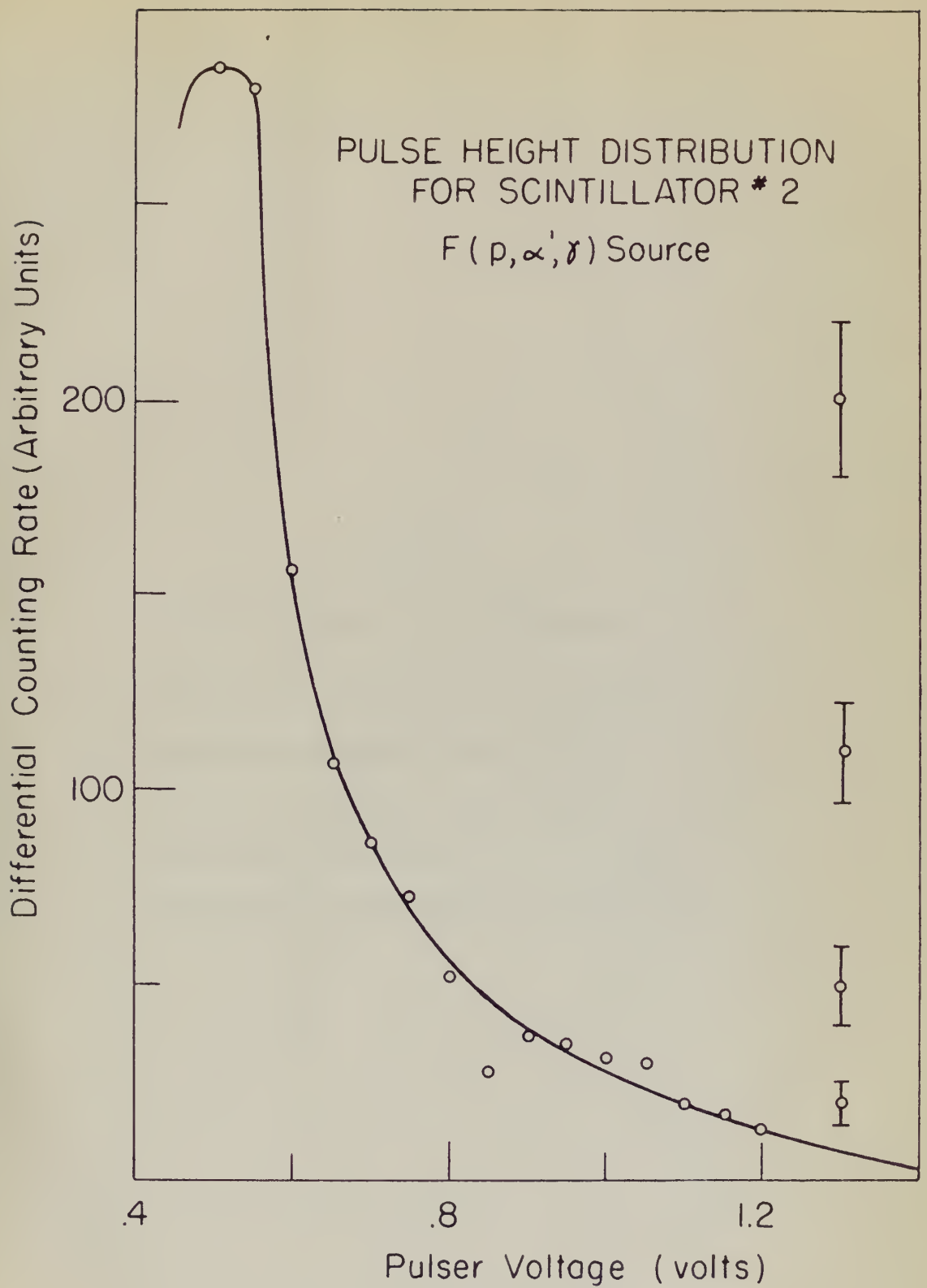
PULSE HEIGHT DISTRIBUTION
FOR SCINTILLATOR # 2
F (p, α', γ) Source
Differential Counting Rate (Arbitrary Units)
200
100
.4
.8
1.2
Pulser Voltage (volts)

Figure 15

Effect of Changing Discriminator No. 1

All curves in this figure were obtained by proton bombardment of a thick CaF target using a 16-mil lead converter. These curves are normalized to the same number of protons incident on the target.

Figure 15

Sites of Dumping Overburden No. 1

All courses in Data Figure were obtained
by persons boardinghouse or a block out
burpit using a 15-mil land surveyor.
These courses are associated to the mean
number of previous incident on the burpit.

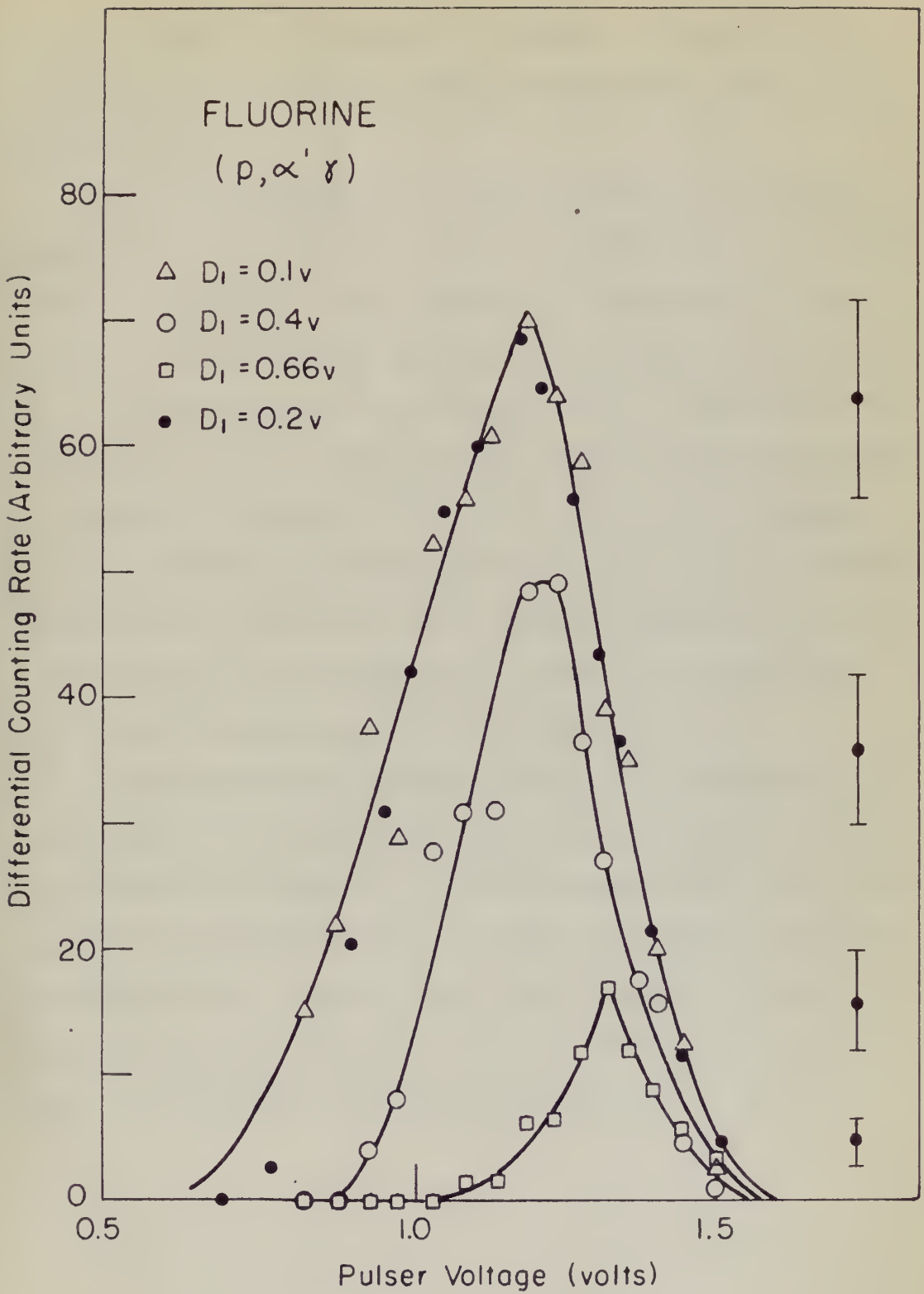
FLUORINE
(p,α'γ)
△ D1 = 0.1v
○ D1 = 0.4v
□ D1 = 0.66v
● D1 = 0.2v
Differential Counting Rate (Arbitrary Units)
0
20
40
60
80
0.5
1.0
1.5
Pulser Voltage (volts)

low to 0.2 volts does not affect the position of the peak or the resolution. D1 at 0.2 volts requires at least 1-Mev energy loss in scintillator No. 1.

Figure 16 illustrates the change in efficiency of the spectrometer with changes in the setting of discriminator No. 2 at 6-Mev incident x-ray energy. These curves were all made with the same setting of D1; that is, 0.2 volts, and normalized to the same number of protons incident on the $F^{19}(p,\alpha'\gamma)$ target. Hence, the ratio of the areas under the curves of Figure 16 gives directly the ratio of spectrometer efficiency for the given discriminator settings. These ratios are 1:2:3.8, in agreement with the shape of the distribution curve for scintillator No. 2 shown in Figure 14. The curve for D2 = 0.8 volts corresponds to an efficiency of 8×10^{-3} for 6-Mev incident x-ray energy, 16-mil lead converter.

Considering the contribution of the 7-Mev fluorine line, the resolution at 6 Mev is about 25 percent, which is about the resolution predicted in Chapter V. The lowest energy at which the present spectrometer is useful is 6 Mev. To reduce this limit, to improve the resolution at 6 Mev, and perhaps more important to obtain a better plateau of efficiency as a function of D2 would require a thinner lead converter and a thinner scintillator No. 2.

low to 0.2 volts does not affect the position of the peak or the resolution. It at 0.2 volts requires at least 1-kev energy loss in scintillator No. 1.

Figure 16 illustrates the change in efficiency of the spectrometer with changes in the setting of discriminator No. 2 at 6-Mev incident x-ray energy. These curves were all made with the same setting of D1, that is, 0.2 volts, and normalized to the same number of protons incident on the $F^{19}(p,\alpha\gamma)$ target. Hence, the ratio of the areas under the curves of Figure 16 gives directly the ratio of spectrometer efficiency for the given discrimination settings. These ratios are 1:3:5, in agreement with the shape of the distribution curve for scintillator No. 2 shown in Figure 15. The curve for D2 = 0.8 volts corresponds to an efficiency of 8×10^{-3} for 6-Mev incident x-ray energy, 16-coil load geometry.

Considering the contribution of the 7-Mev Fluorine line, the resolution at 6 Mev is about 8% percent, which is about the resolution predicted in Chapter V. The lowest energy at which the present spectrometer is useful is 6 Mev. To reduce this limit, to improve the resolution at 6 Mev, and perhaps more important to obtain a better plateau of efficiency as a function of D2 would require a thinner lead converter and a thinner scintillator No. 2.

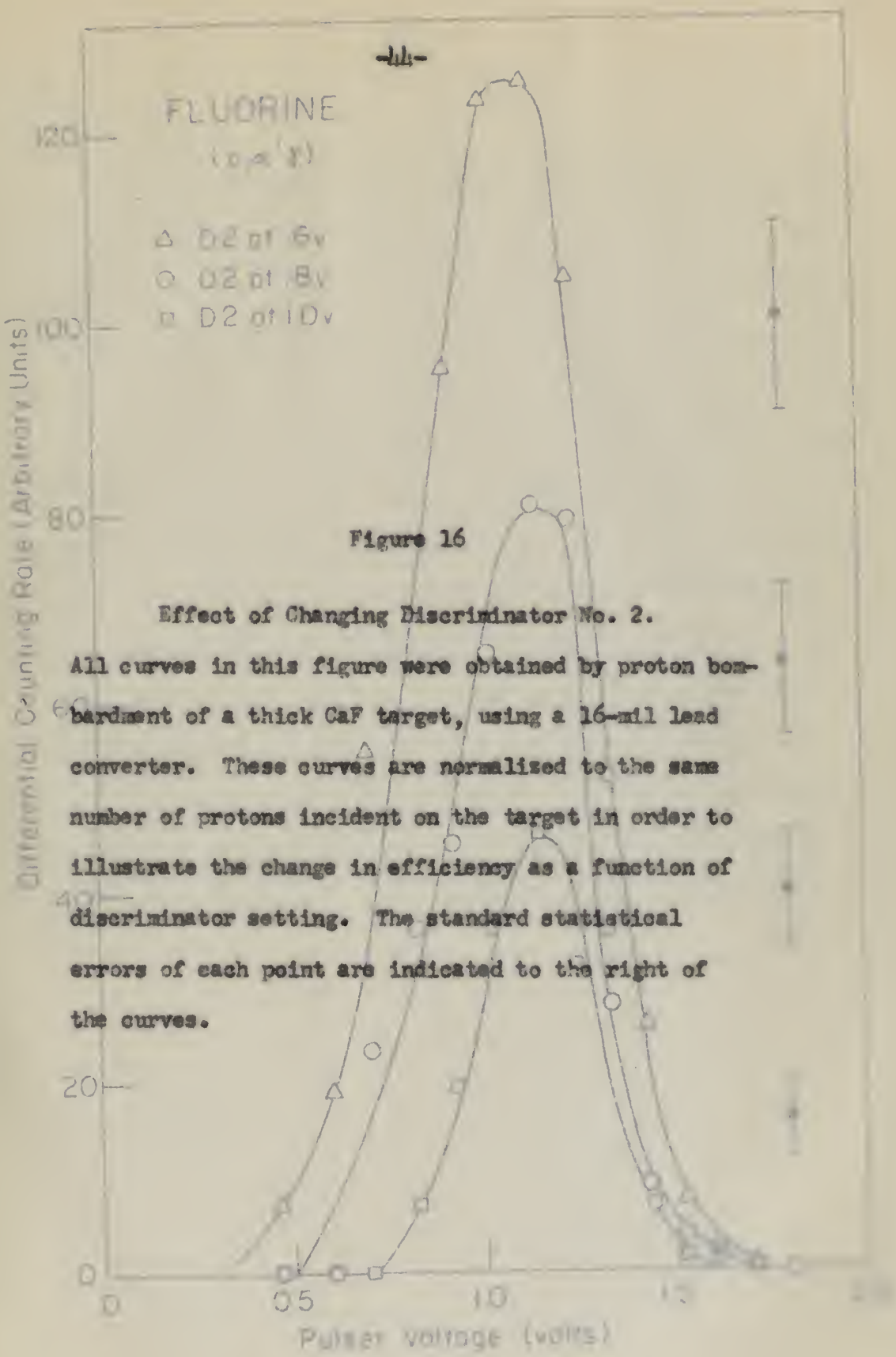

Figure 16

Effect of Changing Discriminator No. 2.

All curves in this figure were obtained by proton bombardment of a thick CaF target, using a 16-mil lead converter. These curves are normalized to the same number of protons incident on the target in order to illustrate the change in efficiency as a function of discriminator setting. The standard statistical errors of each point are indicated to the right of the curves.

Figure 16

Effect of Changing Discriminator No. 2.

All curves in this figure were obtained by proton bombardment of a thick CaF target, using a 16-mil lead converter. These curves are normalized to the same number of protons incident on the target in order to illustrate the change in efficiency as a function of discriminator setting. The standard statistical errors of each point are indicated to the right of the curves.

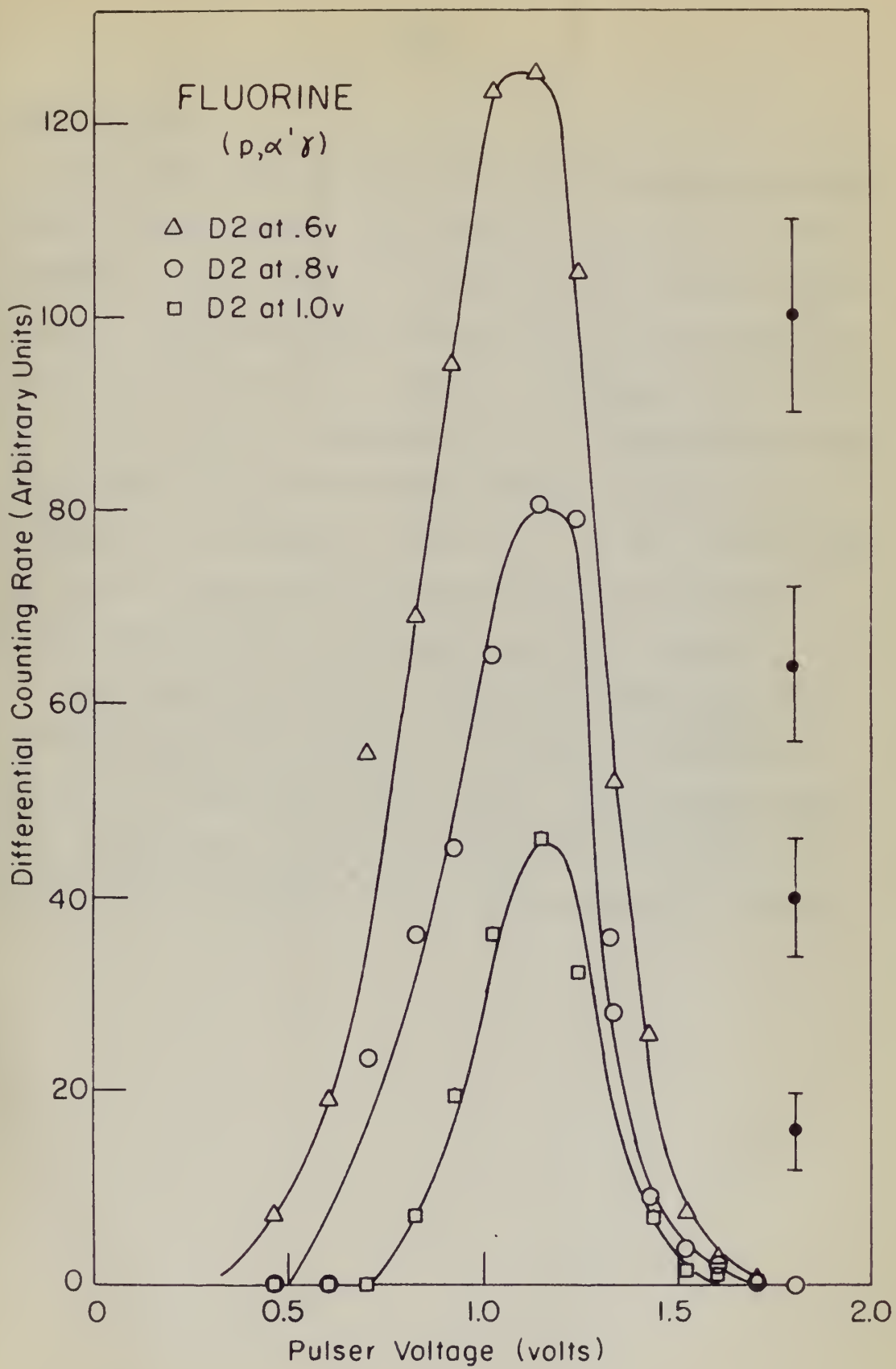
FLUORINE
(p,α'γ)
△ D2 at .6v
○ D2 at .8v
□ D2 at 1.0v
Differential Counting Rate (Arbitrary Units)
120
100
80
60
40
20
0
0
0.5
1.0
1.5
2.0
Pulser Voltage (volts)

HIGH-ENERGY RUNS

The difficulties apparent in the high-energy region, as illustrated by Figure 13, led to the necessity for design of the anticoincidence circuit. Figure 17 illustrates the difficulty in distinguishing singly and doubly ionising events with the anticoincidence scintillator out of the circuit. This figure also demonstrates the apparent success of scintillator No. 3 in eliminating high background effects which mask the expected doubly ionising peak calculated and shown on Figure 9 of Chapter III. To date, the only runs made with the anticoincidence unit in operation were the pulse-height distribution in scintillator No. 2 shown in Figure 17.

The prediction in Chapter V regarding electron escape and radiation loss from scintillator No. 1 should be experimentally verified by a high-energy electron source. The high-energy limit of the spectrometer is imposed as a result of rapidly increasing electron escape probability with increasing energy above 15 Mev.

HIGH-ENERGY BEAM

The difficulties apparent in the high-energy region, as illustrated by Figure 13, led to the necessity for design of the multicathode electrode. Figure 17 illustrates the difficulty in distinguishing singly and doubly ionizing events with the anticoincidence antiutilizer out of the circuit. This figure also demonstrates the apparent success of antiutilizer No. 3 in eliminating high background effects which mask the connected doubly ionizing peak obtained and shown on Figure 9 of Chapter III. To date, the only runs made with the anticoincidence unit in operation were the pulse-height distribution in antiutilizer No. 3 shown in Figure 17.

The modulation in Chamber V separating electron sample and radiation loss from antiutilizer No. 1 should be experimentally verified by a high-energy electron source. The high-energy limit of the spectrometer is imposed as a result of rapidly increasing electron escape probability with increasing energy above 15 Bev.

Figure 17

Effect of the Anticoincidence Circuit at 17 Mev
The curves shown were obtained by proton bombardment of a thick lithium metal target, using a 16-mil lead converter. The need for the anticoincidence circuit at high x-ray energy is illustrated.

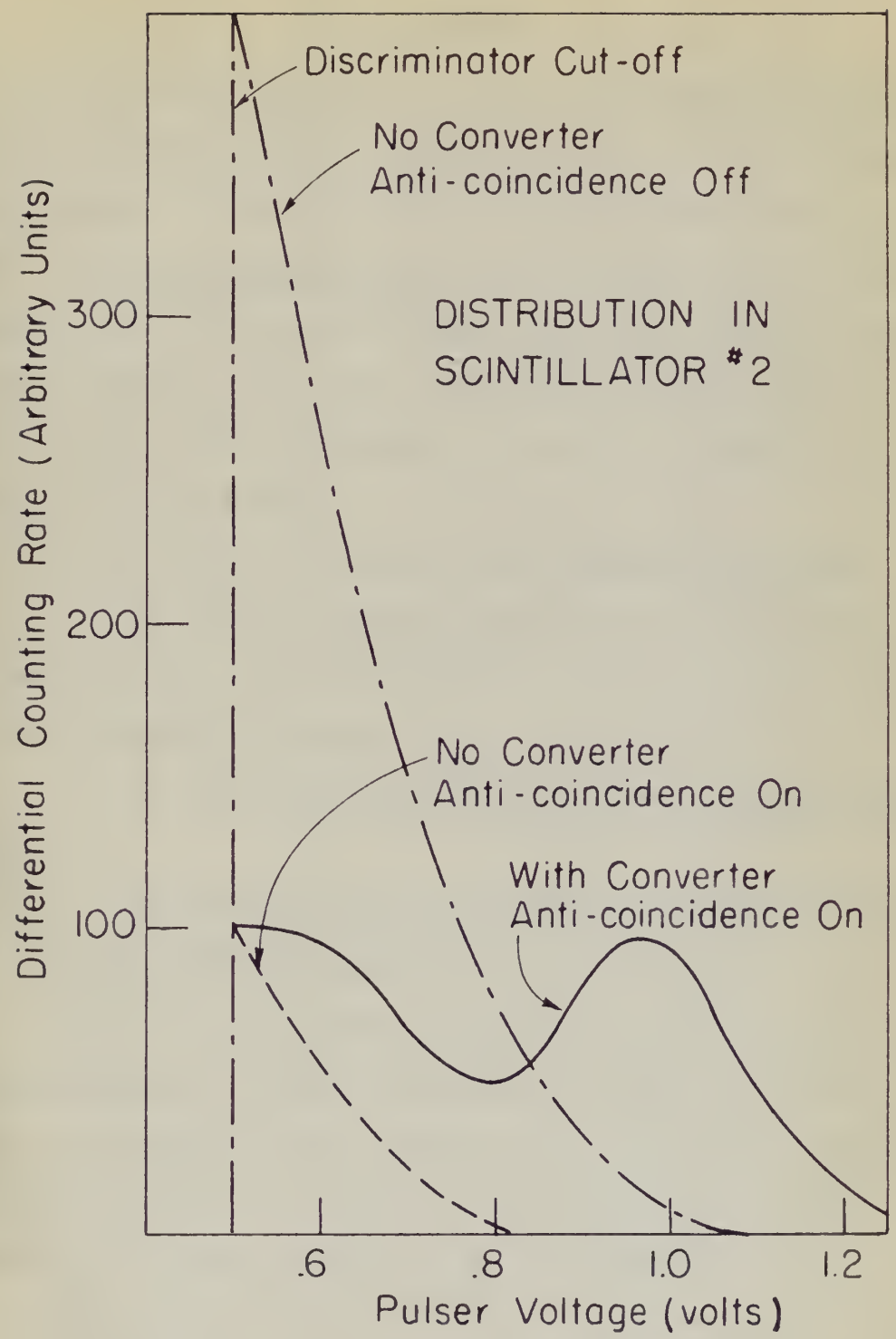
Discriminator Cut-off
No Converter
Anti-coincidence Off
DISTRIBUTION IN
SCINTILLATOR #2
No Converter
Anti-coincidence On
With Converter
Anti-coincidence On
Differential Counting Rate (Arbitrary Units)
300
200
100
.6
.8
1.0
1.2
Pulser Voltage (volts)

VIII. SUMMARY

An attempt has been made to design, instrument, and calibrate an x-ray scintillation pair spectrometer capable of 10 percent resolution at 10 Mev. The spectrometer is designed for use at the M. I. T. linear accelerator and consequently must span the 5- to 17-Mev x-ray energy region. This three scintillator telescope arrangement relies on the ability of a thin plastic scintillator to distinguish the doubly ionizing pulses originating in the thin lead converter as a result of the pair process.

Careful study of the 6-Mev fluorine gamma-ray has shown:

1. That the observed resolution of 20 to 25 percent is in agreement with predicted values for the thickness of the lead converter and plastic scintillator used;

2. That coincidence pulses are doubly ionizing events, and;

3. Better resolution can be obtained by using a thinner lead converter and thinner plastic scintillator No. 2.

Study of the high-energy incident x-ray region, using the 17-Mev lithium gamma-ray, demonstrated that an anticoincidence circuit was necessary to distinguish doubly ionizing events. Subsequent experimental observations of the pulse height distribution in scintillator No. 2 pointed to the apparent success of the anticoincidence circuit. A program similar to that performed at 6 Mev remains to be carried out at 17 Mev to determine optimum operating conditions in this energy region.

VIII. SUMMARY

An attempt has been made to design, construct, and calibrate an x-ray calorimeter pair spectrometer capable of 10 percent resolution at 10 Mev. The spectrometer is designed for use at the M. I. T. linear accelerator and consequently must span the 5- to 17-Mev x-ray energy region. This three calorimeter telescope arrangement relies on the ability of a thin plastic scintillator to distinguish the doubly ionizing pairs originating in the thin lead converter as a result of the pair process.

Careful study of the 6-Mev Zinnia x-ray beam has shown:

1. That the observed resolutions of 20 to 25 percent is in agreement with predicted values for the thicknesses of the lead converter and plastic scintillator used;

2. That coincidences pulses are doubly ionizing events; and;

3. Energy resolution can be obtained by using a thinner lead converter and thinner plastic scintillator No. 2.

Study of the high-energy incident x-ray region, using the 17-Mev Mitchie pencil-ray, demonstrated that an anticoincidence circuit was necessary to distinguish doubly ionizing events. Subsequent experimental observations of the pulse height distribution in scintillator No. 2 pointed to the apparent success of the anticoincidence circuit. A procedure similar to that performed at 6 Mev remains to be carried out at 17 Mev to determine optimum operating conditions in this energy region.

APPENDIX I

CALCULATION OF DIFFERENTIAL ENERGY LOSS DISTRIBUTION FOR SCINTILLATOR No. 2 AT 17.6-Mev INCIDENT X-RAY ENERGY

Using the electron energy distributions given by Johns et al[24] in tabulated form for 1-Mev energy intervals (17.6-Mev incident x-ray energy) and the angular distribution in terms of the electron energy, it is possible to calculate a theoretical energy loss distribution curve for scintillator No. 2 in the following manner. The angle a Compton recoil electron makes with the incident photon is fixed for a given photon energy by the relation[25]

$$\tan^2 \phi_E = \frac{2\alpha(\gamma/E - 1) - 1}{(1 + \alpha)^2}$$

where γ = energy of incident photon in Mev;

E = energy of recoil electron;

$\alpha = \gamma/mc^2$;

mc^2 = electron rest mass, 0.51 Mev.

The average angle between the direction of motion of a created electron (positive or negative) and of the photon is[9]

$$\theta_0 = \frac{mc^2}{E}$$

where E is the energy of the electron.

APPENDIX 2

CALCULATION OF EXPERIMENTAL ENERGY LOSS SPECTRUM FOR SCINTILLATOR No. 2 AT 17.6-MeV INCIDENT X-RAY ENERGY

Using the electron energy distribution given by Jelley et al[8] in integrated form for 1-MeV energy intervals (17.5-MeV incident x-ray energy) and the angular distribution in terms of the electron energy, it is possible to calculate a theoretical energy loss distribution curve for scintillator No. 2 in the following manner. The angle a Compton recoil electron makes with the incident photon is fixed for a given photon energy by the relation[29]

$$\tan^2\phi_e = \frac{2(\epsilon/\epsilon + 1) - 1}{(1+\epsilon)^2}$$

where ϵ = energy of incident photon in MeV;

ϕ_e = recoil electron angle;

$\epsilon = h\nu/mc^2$;

mc^2 = electron rest mass, 0.51 MeV.

The energy split between the direction of motion of a recoiled electron (positive or negative) and of the photon is[8]

$$\delta_1 = \frac{1-\epsilon}{1+\epsilon}$$

where δ is the energy of the electron.

Once the electron enters the scintillator, it no longer travels in its initial direction given by ϕ_g or θ_o, but is subjected to single and multiple scattering. One method of finding the actual path length of electrons has been discussed by Yang[26]. Yang uses a correction Δ such that $t' = t + \Delta$, where t' is the actual path length and t is the foil thickness measured in radiation lengths[27].

$$\Delta_{average} = \frac{t^2 E_s^2}{4P^2\beta^2} ,$$

where E_s = characteristic energy = 21.2 Mev;

P = electron momentum in Mev;

β = velocity of electron in units of the velocity of light.

This result was derived from the gaussian approximation of Rossi[27] but could be obtained from the exact numerical solution of Snyder and Scott[28]. It is felt that the gaussian approximation is of reasonable accuracy for these calculations and will be used throughout this paper when investigating multiple scattering effects. Using the above formula and the collision loss as a function of energy given in Johns et al[24], it was possible to prepare the histogram shown in Figure 9 for the 17.6-Mev lithium gamma-ray.

The Compton cross section at 17.6 Mev was obtained from Davisson and Evans[25]; but, since the observed pair production cross sections

Once the electrons reach the ionization, it no longer
travels in the initial direction given by $\vec{P}_0$ or θ_0, but is accelerated to atomic and molecular velocities. One method of finding the actual path length of electrons has been discussed by Lang[24]. There must a correction Δ such that $t' = t + \Delta$, where t' is the actual path length and t is the full distance measured in radiation lengths[27].

$$\Delta_{average} = \frac{E_c^2 t}{E_T^2 \beta^2} ,$$

where E_c = characteristic energy = 21.2 Mev;

T = electron momentum in Mev;

β = velocity of electrons in units of the velocity of light.

This result was derived from the gaussian approximation of Rossi[27] but could be obtained from the exact numerical solution of Snyder and Scott[28]. It is felt that the gaussian approximation is of reasonable accuracy for these calculations and will be used throughout this paper when investigating multiple scattering effects. Using the above formula and the collision loss as a function of energy given in Jones et al[29], it was possible to produce the histogram shown in Figure 9 for the 17.6-Mev lithium gamma-ray.

The doughnut cross section at 17.6 Mev was obtained from Davison and Evans[25], but since the observed pair production cross sections

for lead above 5 Mev differ as much as 10 percent from the calculated values, the value for the pair cross section was the experimental value obtained by Walker[29].

The energy loss of the electrons in the converter has not been taken into account in any of the curves shown in Figure 9. Hough[30] gives the probability of emission at an angle greater than θ_1 (for large angles) as roughly:

$$3/8 \left(\frac{mc^2}{E}\right)^2 \quad \frac{1}{1 - \cos \theta_1}$$

where E is the energy of the observed electron. From this, it can be seen that the actual pair angular distribution will spread the energy loss in scintillator No. 2 out towards the higher energy (longer actual path length). The finite resolution of the photomultiplier will spread the distribution out on both sides of the peak. The resulting qualitative curve is shown in Figure 9.

for land above 7 the differ as much as 10 percent from the calculated values, the value for the air-ocean boundary was the experimental value obtained by Eckart[7].

The energy loss of the electrons in the ionosphere has not been taken into account in any of the curves shown in Figure 9. Though[30] gives the probability of scattering at an angle greater than θ_1 (for large angles) as proportional to

$$\frac{1}{1 - \cos\theta_1} \left(\frac{mc^2}{E}\right)^2$$

where E is the energy of the incident electrons. From this, it may be seen that the actual path length of the electrons will exceed the energy loss in proportion to E. I was assumed the higher energy (longer actual path length). The total reflection of the ionosphere will depend on the characteristics and on both sides of the path. The resulting qualitative curve is shown in Figure 9.

BIBLIOGRAPHY

1. H. W. Koch and R. S. Foote, Phys. Rev. 91, 455 (1953).

2. J. L. Burkhardt, Ph.D. Thesis, M.I.T., February 1955.

3. H. W. Koch and R. S. Foote, Rev. Sci. Inst. 25, 746 (1954).

4. R. L. Walker and B. D. McDaniel, Phys. Rev. 74, 315 (1948).

5. B. B. Kinsey and G. A. Bartholomew, Can. J. Phys. 31, 537 (1953).

6. R. R. Carlson et al, Phys. Rev. 94, 1311 (1954).

7. J. K. Bair and F. C. Maienschein, Rev. Sci. Inst. 22, 343 (1951).

8. S. A. E. Johansson, Nature 166, 794 (1950); Phil. Mag. (London) 43. 249 (1952).

9. Segre, Experimental Nuclear Physics, Vol. I (1953), John Wiley and Sons (New York).

10. R. K. Swank, Annual Review Nuclear Science 4, 111 (1954).

11. T. Huus and R. B. Day, Phys. Rev. 91, 599 (1953).

12. R. L. Walker, Phys. Rev. 79, 172 (1950).

13. H. Mark and G. Goldring, Rockefeller Generator Group, M.I.T., private communication.

14. J. G. Campbell and A. J. F. Boyle, Australian J. Phys, 6, 171 (1953).

15. W. Heitler, The Quantum Theory of Radiation, Clarendon Press, Oxford (1936).

16. W. A. Fowler and C. C. Lauritsen, Phys. Rev. 76, 314 (1949).

17. C. N. Chou, Phys. Rev. 87, 376 (1952).

1. W. E. Cook and R. B. Peake, Phys. Rev. 71, 675 (1947).

2. W. L. Hartshorn, M.S. Thesis, M.I.T., February 1956.

3. H. T. Cook and E. E. Fowler, Rev. Mod. Instr. 25, 746 (1954).

4. E. L. Kothen and J. L. Hollenhal, Phys. Rev. 76, 1037 (1949).

5. R. H. Dicke and C. A. Barthalomew, Chm. & Phys. 21, 5317 (1953).

6. R. E. Cleveland et al, Phys. Rev. 91, 1313 (1953).

7. G. E. Hale and F. O. Rasmussen, Rev. Sci. Inst. 25, 343 (1953).

8. J. A. K. Adamson, Nature 166, 738 (1950); 1613. Eng. (London) 43, 819 (1952).

9. Zeppe, Instrument Engineer Practice, Vol. I (1953), John Wiley and Sons (New York).

10. E. Gross, Journal Applied Physics Volume 5, 233 (1954).

11. T. Dunn and F. T. Loy, Phys. Rev. 93, 998 (1954).

12. E. L. Talbert, Phys. Rev. 77, 272 (1950).

13. R. Mark and D. Calvert, Precision Electronic Instruments, M.I.T., unpublished communication.

14. C. O. Cawthorn and A. G. F. Hoyle, Australian J. Phys, 6, 172 (1953).

15. R. Dutton, The Inverse Theory of Inductions, Clarendon Press, Oxford (1934).

16. W. A. Fowler and C. C. Lauritsen, Phys. Rev. 76, 314 (1949).

17. C. E. Cleeton, Phys. Rev. 57, 345 (1940).

18. L. Katz and A. S. Penfold, Revs. Modern Phys. 24, 28 (1952).

19. Pilot Chemical Company, Waltham, Massachusetts.

20. S. Janes, Synchrotron Laboratory, M. I. T., private communication.

21. K. H. Spring, Photons and Electrons, John Wiley and Sons, New York (1950).

22. R. D. Evans, The Atomic Nucleus, McGraw-Hill, to be published.

23. R. M. Sternheimer, Phys. Rev. 88, 851 (1952).

24. H. E. Johns et al, Nucleonics, 12, 40 (1954).

25. C. M. Davisson and R. D. Evans, Revs, Modern Phys. 24, 79 (1952).

26. C. N. Yang, Phys. Rev. 84, 599 (1951).

27. B. Rossi and K. Greisen, Revs. Modern Phys. 13, 240 (1941).

28. H. Snyder and W. T. Scott, Phys. Rev. 76, 220 (1949).

29. R. L. Walker, Phys. Rev. 76, 527 (1949).

30. P. V. C. Hough, Phys. Rev. 74, 80 (1949).

31. R. K. Swank and W. L. Buck, Nucleonics 10-5, 51 (1952).

32. B. R. Linden, Nucleonics 11-9, 30 (1953).

33. J. Saldick and A. O. Allen, J. Chem. Phys. 22, 438 (1954).

34. H. A. Bethe and W. Heitler, Proc. Roy. Soc. (London), A146, 83 (1934).

35. L. Eyges, Phys. Rev. 77, 81 (1950).

36. E. S. Rosenblum, AECU Report No. 1825 (1951).

37. W. Paul and H. Reich, Z. Physik 127, 429 (1950).

38. J. J. S. Chen and S. D. Warshaw, Phys. Rev. 84, 355 (1951).

39. Goldwasser et al, Phys. Rev. 88, 1137 (1952).

40. L. Landau, J. Phys. USSR) 8, 201 (1944).

41. Fano, Nucleonics, 11-8, 8 (1953).

Th
S6628 Snyder 28794
Instrumentation and calibration of X-ray scintillation pair spectrometer.